

# Functional roles of tyrosine 185 during the bacteriorhodopsin photocycle as revealed by *in situ* spectroscopic studies\*\*

Xiaoyan Ding<sup>1,2,‡</sup>, Chao Sun<sup>1,‡</sup>, Haolin Cui<sup>1</sup>, Sijin Chen<sup>1</sup>, Yujiao Gao<sup>1</sup>, Yanan Yang<sup>1</sup>, Juan Wang<sup>1</sup>, Xiao He<sup>3</sup>, Dinu Iuga<sup>4</sup>, Fang Tian<sup>2,\*</sup>, Anthony Watts<sup>5,\*</sup> and Xin Zhao<sup>1,\*</sup>

<sup>1</sup>Shanghai Key Laboratory of Magnetic Resonance, Department of Physics, East China Normal University, Shanghai 200062, P.R. China

<sup>2</sup>Department of Biochemistry and Molecular Biology, Penn State College of Medicine, PA 17033-0850, USA

<sup>3</sup>Department of Chemistry, East China Normal University, Shanghai 200062, P.R. China

<sup>4</sup>The UK 850 MHz Solid-State NMR Facility, Department of Physics, University of Warwick, Coventry CV4 7AL, UK

<sup>5</sup>Department of Biochemistry, University of Oxford, South Parks Road, Oxford OX1 3QU, UK

<sup>‡</sup>These authors contributed equally to this work.

\*Corresponding authors:

Shanghai Key Laboratory of Magnetic Resonance, Department of Physics; East China Normal University, Shanghai 200062, PR China. Tel.: +86-21-62234329; Fax: +86-21-62234329; Email: xzhao@phy.ecnu.edu.cn

Department of Biochemistry, University of Oxford, South Parks Road, Oxford OX1 3QU, UK. Tel.: +44-1865-613219; Fax: +44-1865-613201; Email: anthony.watts@bioch.ox.ac.uk

Department of Biochemistry and Molecular Biology, Penn State College of Medicine, PA 17033-0850, USA. Tel.: +1-717-531-8585; Fax: +1-717-531-7072; Email: ftian@psu.edu

\*\*This article contains Supplementary material.

## **ABSTRACT**

Tyrosine 185 (Y185), one of the aromatic residues within the retinal (Ret) chromophore binding pocket in helix F of bacteriorhodopsin (bR), is highly conserved among the microbial rhodopsin family proteins. Many studies have investigated the functions of Y185, but its underlying mechanism during the bR photocycle remains unclear. To address this research gap, *in situ* two-dimensional (2D) magic-angle spinning (MAS) solid-state NMR (ssNMR) of specifically labelled bR, combined with light-induced transient absorption change measurements, dynamic light scattering (DLS) measurements, titration analysis and site-directed mutagenesis, was used to elucidate the functional roles of Y185 during the bR photocycle in the native membrane environment. Different interaction modes were identified between Y185 and the Ret chromophore in the dark-adapted (inactive) state and M (active) state, indicating that Y185 may serve as a rotamer switch maintaining the protein dynamics, and plays an important role in the efficient proton-pumping mechanism in the bR purple membrane.

## **KEYWORDS**

Tyrosine 185; retinal chromophore; dark-adapted state and M state; photocycle; proton pumping

## 1. Introduction

Microbial rhodopsins are one of the largest groups of photoreceptors that include bacteriorhodopsin (bR), anabaena sensory rhodopsin (aSR), proteorhodopsin (pR), archaerhodopsins (aRs), xanthorhodopsin (xR), channelrhodopsin-2 (chR2) and halorhodopsin (hR), and they share a common seven-transmembrane (TM) helical topology with a light-sensitive retinal (Ret) chromophore covalently bound to a lysine (K) residue in helix G via a protonated Schiff base (SB) linkage [1-9]. While they perform a similar photo-induced cascade chemical reaction, diverse functions are executed by different microbial rhodopsins, such as ion pumps, channels and photosensors [10, 11].

bR, a light-driven proton pump found in the purple membrane of *Halobacterium salinarum*, was the first microbial rhodopsin photoreceptor to be discovered and has served as an ideal model for the study of other microbial rhodopsins [12-14]. In the dark-adapted (DA) state, 13-*cis*, 15-*syn* Ret (denoted as bR<sub>cis</sub>) and all-*trans*, 15-*anti* Ret (denoted as bR<sub>trans</sub>), are thermally interconvertible, with a molar ratio close to 1:1 (Fig. 1A) [15-19]. Photo-isomerization of the Ret chromophore from the all-*trans* to the 13-*cis* configuration triggers a cyclic reaction that includes a series of K-, L-, M-, N- and O-like photo-intermediates to transfer a proton vectorially across the cell membrane (Supplementary material Fig. S1) [20]. Tyrosine 185 (Y185), one of the aromatic residues within the Ret binding pocket in helix F of bR (Fig. 1B), is one of the most conserved residues among the microbial rhodopsin family proteins (Table S1) [11]. Early studies have shown that Y185 might play an important role in stabilizing the pentagonal hydrogen-bond (H-bond) network on the extracellular side of the SB and might be involved in the reprotonation of the SB during the early stage of the photocycle [21, 22]. Our recent studies demonstrated that Y185 plays a role in maintaining the twisted polyene chain of the Ret chromophore and stabilizing the Ret *cis-trans* isomerization thermal equilibrium in the DA state [23, 24]. Removal of the phenolic hydroxyl in the Y185F mutant shifts the *cis-trans* equilibrium to a bR<sub>cis</sub>-dominated state and affects the

photocycle kinetics of bR [23, 24]. Aromatic residues are well known to be highly conserved in G-protein-coupled receptors (GPCRs) and play very important roles in activating the global toggle switch through a local micro-switch mechanism [25-29]. For example, tyrosine 306 (Y306) of the NPxxY motif in TM-VII of rhodopsin participates in global activation by undergoing a transition between the two different rotamer conformations upon receptor activation, which opens a continuous internal water channel for rhodopsin activation [30]. Such a rotamer switch mechanism not only exists in rhodopsin but also occurs in other GPCRs, such as  $\beta_1$ - and  $\beta_2$ -adrenergic receptors,  $A_{2A}$  adenosine receptor, and squid rhodopsin [31-35]. However, a similar function for an aromatic residue has never been reported in microbial rhodopsin family proteins. Therefore, as an example, an understanding of the functional roles of Y185 during the bR photocycle is necessary to verify the mechanism by which it modulates the proton-pumping capability and helps provide mechanistic insights into the aromatic residues for other microbial rhodopsins.

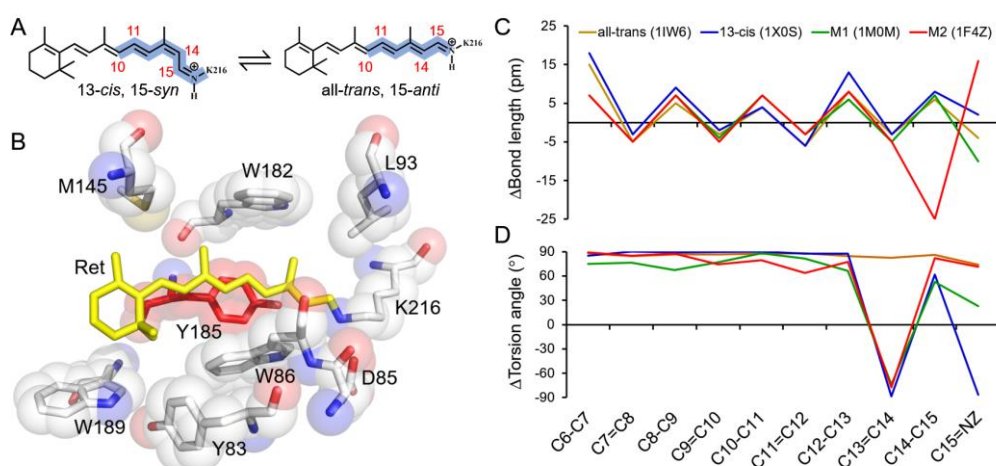


**Figure 1.** *Cis-trans* thermal equilibrium of Ret in the DA state of bR (A); Crystal structure of the Ret binding pocket, highlighting Y185 and other key residues (PDB code: 1C3W) (B) [36]; Bond length (C) and torsion angle (D) alternations of the Ret sidechain in the bR<sub>cis</sub> (blue), bR<sub>trans</sub> (brown), M<sub>1</sub> (green) and M<sub>2</sub> (red) states obtained from the crystal structures of bR (1X0S, 1IW6, 1M0M and 1F4Z) [37, 38].

In this study, we exploited *in situ* two-dimensional (2D) magic-angle spinning (MAS) solid-state NMR (ssNMR) to address the molecular mechanisms underlying the interactions between Y185 and the Ret chromophore in the DA state and

photoactive M states in their native membrane environment. Light-induced transient absorption change measurements, dynamic light scattering (DLS) measurements, titration analysis and site-directed mutagenesis were combined to elucidate the functional roles of Y185 during the bR photocycle. Different interaction modes were identified between Y185 and the Ret chromophore in the DA state and M states. In addition, a shifted Ret *cis-trans* isomerization thermal equilibrium, a deficient photocycle, and unfavourable trimeric assembly dynamics and energy conversion were observed in the Y185F-bR. Our results demonstrated that Y185 may serve as a rotamer switch, maintaining the protein dynamics with a rigid conformation through a SB N–H···OH–Y185 H-bond in the DA state and a flexible conformation via release of this H-bond and drift of the aromatic ring of the Y185 away from the Ret in the M states, and plays an important role in the directional transfer of the proton.

## 2. Materials and Methods

### 2.1 Expression of recombinant Y185F

The *bop* gene fragment containing 5' and 3' flanking regions was cloned into the *E. coli* plasmid vector pUC19 to produce the shuttle plasmid pUC19-*bop*. A point mutation at Y185 to phenylalanine (F) was introduced into the *bop* gene by the inverse PCR method using the following two primers: 5'-GTGGTCCGCGTTTCCCGTCGTGTG-3', and 5'-CACACGACGGGAAACGCGGACCAC-3'. The Y185F mutated *bop* gene was then amplified and subcloned into the expression vector to yield pXLNor-Y185F-*bop* plasmid, and then the recombinant plasmid was transformed into the *bop* deficient strain (*bop*<sup>-</sup>) *H. salinarum* L33 to produce the corresponding protein, denoted as Y185F<sup>L33</sup>-bR (Y185F-bR). In the same way, the wild-type (WT) bR expressed in the strain of R1M1 is denoted as WT<sup>R1M1</sup>-bR (WT-bR). The screened strains were then cultured on a large scale for further expression and purification, and the purple product was harvested. A sucrose gradient with concentrations of 35%, 43% and 60% (w/w) was used for purification of the native membrane according to the standard procedures [39]. The concentration of the purified protein was determined by using the Bradford method [40, 41], and was cross checked using

the extinction coefficient of  $62,700 \pm 700 \text{ M}^{-1}\text{cm}^{-1}$  at the absorption maximum of 568 nm [42]. The molecular weight of the recombinant Y185F<sup>L33</sup>-bR was determined by SDS-PAGE, and Ret binding in WT<sup>R1M1</sup>-bR and Y185F<sup>L33</sup>-bR was examined by UV–VIS absorption spectroscopy. <sup>13</sup>C- and <sup>15</sup>N-labelled WT<sup>R1M1</sup>-bR and Y185F<sup>L33</sup>-bR purple membranes were prepared with synthetic media, in which the unlabelled tyrosine and phenylalanine were replaced by isotope-labelled amino acids [43].

## 2.2 Solid-state NMR experiments

All solid-state NMR measurements were performed on either a Bruker 600 MHz Avance III wide bore spectrometer at  $-25 \pm 1$  °C or on a Bruker 850 MHz Avance III wide bore spectrometer at  $-65 \pm 1$  °C. Either a 3.2-mm or a 4.0-mm probe configured in double resonance or triple resonance mode was used with a MAS spinning frequency of 8-16 kHz for different experiments. In all experiments, a ramped cross-polarization (CP) [44] with a 90–100% linear gradient was used with a radiofrequency (rf) field of 50 kHz on the proton channel. Typical 90° rf pulse lengths were 3.8  $\mu\text{s}$  for <sup>13</sup>C and 2.7  $\mu\text{s}$  for <sup>1</sup>H channels. The two-pulse phase modulation (TPPM) [45] with a pulse width of 5.5-6  $\mu\text{s}$  for proton decoupling was used throughout the experiments. A recycle delay of 3 s was set for all the experiments. A 100 or 500 ms mixing time with proton-driven spin-diffusion (PDSD) or dipolar-assisted rotational resonance (DARR) schemes [46, 47] was employed in the 2D <sup>13</sup>C–<sup>13</sup>C correlation experiments. The POST-C7 sequence [48] with an rf field of 56 kHz for the double quantum excitation and reconversion, and a continuous wave decoupling at the Lee-Goldburg condition (CWLG) [49] of 85 kHz was applied during the Post-C7 was used for the double-quantum filtration (DQF) experiments. The <sup>13</sup>C chemical shifts were referenced to the methylene peak of adamantane [50], and the <sup>15</sup>N chemical shifts were referenced indirectly by using the gyromagnetic ratio of  $\gamma_{\text{N}}/\gamma_{\text{C}} = 0.402979940$  [51].

Preparation of the DA state samples: The labelled bR purple membrane samples were suspended in a buffer with 25 mM NaCl, 10 mM HEPES, 0.025% (w/w) NaN<sub>3</sub> at

pH 7, packed into different 3.2 mm zirconia rotors and incubated for 2 days before running NMR experiments.

Preparation of the M state samples: The labelled bR purple membrane samples were prepared with 300 mM Gdn·HCl, 25 mM NaCl, 10 mM CHLS, 0.025% (w/w) NaN<sub>3</sub> at pH 10, packed into different 3.2 mm zirconia rotors and incubated for 2 days. The sample rotors were illuminated with a 1000 W xenon lamp at 0 °C in an ice-water bath for 2 hrs for light-adaptation, and then cooled down to –60 °C with a dry ice ethanol bath and illuminated again for another 3 hrs with the xenon lamp using a 550 nm cut-off filter for accumulation of the M state, similar as reported before [52, 53]. The samples were then quickly transferred into the pre-cooled 3.2 mm probe at –80 °C within 10 seconds to prevent vanishing of the M state, and spun immediately for the NMR measurements. The real temperature on the sample rotors was calibrated with lead nitrate by the standard method [54].

### **2.3 Light-induced transient absorption kinetic spectroscopy**

The proton pumping activities of WT<sup>R1M1</sup>-bR and Y185F<sup>L33</sup>-bR were monitored through light-induced transient absorption changes using the pH-sensitive dye pyranine (8-hydroxy-1, 3, 6-pyrenetrisulfonic acid, trisodium salt) on a homemade apparatus [55]. The kinetics of the M state, the O state and the recovery trajectory to the ground state were monitored at 410 nm, 660 nm and 570 nm, respectively. All experiments were conducted using a photoflash with a half-bandwidth less than 1 ms for excitation. The time constants were extracted through the best fitting of the experimental data with multi-exponential functions. All the samples were in light-adapted conformation and suspended in a buffer with 100 mM NaCl and 20 mM KCl at pH 7.0. All the measurements were performed at room temperature.

### **2.4 Dynamic light scattering measurements**

bR presents a trimeric structure in the purple membrane, and the trimer-membrane interaction is important in controlling the bR photocycle [56]. Since only the protein-containing native membrane fragments, rather than the full band, are obtained by sucrose gradient centrifugation purification [39], the patch

sizes and polydispersity indices of the WT<sup>R1M1</sup>-bR and Y185F<sup>L33</sup>-bR membrane fragments obtained from DLS can be used to characterize the protein assembly conditions. The measurements were performed using the Malvern Zetasizer Nano ZS90 DLS spectrometer (Malvern Instruments, UK) at 20 °C. The samples were diluted with deionized water at pH 7.0 and then adjusted to concentrations of 6 µM, 8 µM and 10 µM. Three parallel samples were measured with 10-30 times average of each one to reduce the experimental error.

## **2.5 Titration of D85**

The complex titration of D85 in the unphotolysed protein has been suggested to reflect the dependence of this residue on the thermal equilibration of the DA Ret and the deprotonation kinetics of the SB during the photocycle [57]. The pH-dependent absorption spectra of the WT<sup>R1M1</sup>-bR and Y185F<sup>L33</sup>-bR were recorded first, and then difference spectra were obtained by subtracting the last absorption curve in each respective plot of the spectrum (Fig. S7). The absorption changes at 660 nm versus pH were then plotted, and the pKa values were extracted using the Henderson–Hasselbalch equation to find the best fitting curves [58]. The absorption spectra of the DA purple membrane were recorded on a UV-VIS spectrophotometer in a pH range of 2 to 7.

## **2.6 ATP formation rate measurements**

The ATP formation rates in the WT<sup>R1M1</sup>-bR and Y185F<sup>L33</sup>-bR cells were measured using a luciferase-based assay (SpectraMax M5/M5e, IRIS II XSP).

The Enhanced ATP Assay Kit (S0027, Beyotime, CN) was used to detect the ATP levels in the cells. Briefly, all of the halophilic cell types were grown in parallel in peptone medium with salts according to the standard method [55] and were harvested after reaching the growth plateau. The cell pellets were then suspended in peptone medium and adjusted to an OD of 0.2 at 660 nm with a final volume of 2 ml and then centrifuged at 12,000 rpm for 1 min (Microfuge<sup>®</sup> 16, Beckman, USA). The cells were subsequently collected and resuspended in lysis buffer. For the measurements, identical amounts of the diluted ATP assay solution were added to



the samples and incubated at room temperature for 3 to 5 minutes. A 20  $\mu$ l sample of an ATP standard solution was added to a plate and mixed sufficiently. The luminescence intensity was monitored with a fluorescence microplate reader after incubation for at least several seconds. An ATP standard curve was first prepared to calculate the ATP concentration of each sample, as shown in Fig. S10.

### 3. Results and Discussion

#### 3.1 Coupling of the Ret-Y185 H-bond in the DA state and photoactive M states in the bR purple membrane

To address the functional roles of Y185 during the bR photocycle, we first focus on the couplings between the Ret polyene chain and aromatic ring of Y185 in the DA state and photoactive M states using *in situ* ssNMR. First, 2D PDSD experiments and one-dimensional (1D) DQF experiments with the POST-C7 sequence were performed using the [10, 11, 14, 15- $^{13}\text{C}_4$ ]-Ret-regenerated bR samples to obtain the chemical shifts (CSs) of Ret at the 10, 11, 14 and 15 sites in the DA state and M states, as shown in Fig. 2 and Table 1. Fig. 2A shows the superimposed 2D  $^{13}\text{C}$ - $^{13}\text{C}$  PDSD correlation spectra of the [10, 11, 14, 15- $^{13}\text{C}_4$ ]-Ret-regenerated WT-bR in the DA (blue) state and M (red) states. Two intensely overlapping crosspeaks between the  $^{13}\text{C}15$  and  $^{13}\text{C}14$  resonances appeared at (164.0, 125.7) ppm and (164.8, 124.0) ppm in the M states, representing an equilibrium of the early M state ( $M_1$ ) and later M state ( $M_2$ ) in the bR purple membrane, similar to that reported previously [52]. No crosspeak was observed between the  $^{13}\text{C}11$  and  $^{13}\text{C}10$  resonances in the M states. However, the row projection of the 2D spectra in the M states showed an unusually intense peak at  $\sim 129.4$  ppm (Fig. 2B). We suggest that this unusually intense peak is due to the merger of the  $^{13}\text{C}11$  resonance with the  $^{13}\text{C}10$  resonance in the M states. A similar resonance assignment has been reported for C11 in the  $M_1$  state with an isolated  $^{13}\text{C}11$ -Ret-labelled bR [59]. Large shifts of 4.0 ppm at C15, 3.0 ppm at C14,  $-6.0$  ppm at C11, and  $-3.8$  ppm at C10 from bR<sub>trans</sub> to  $M_1$ , and 4.8 ppm, 1.3 ppm,  $-6.0$  ppm and  $-3.8$  ppm at those same sites from bR<sub>trans</sub> to  $M_2$  were observed here, suggesting a large rearrangement of the Ret binding pocket upon activation. The

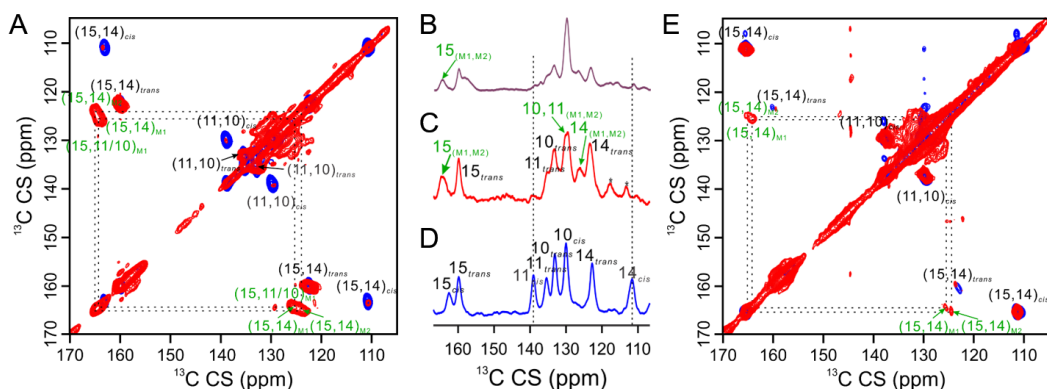


**Figure 2.** Superimposed 2D  $^{13}\text{C}$ – $^{13}\text{C}$  correlation spectra of the [10, 11, 14, 15- $^{13}\text{C}_4$ ]-Ret-regenerated WT-bR in the DA (blue) and M (red) states (A); The row projection of the 2D  $^{13}\text{C}$ – $^{13}\text{C}$  correlation spectrum in the M states (B); 1D DQF spectra of the [10, 11, 14, 15- $^{13}\text{C}_4$ ]-Ret-regenerated WT-bR in the DA (D) and M states (C); Superimposed 2D  $^{13}\text{C}$ – $^{13}\text{C}$  correlation spectra of the [10, 11, 14, 15- $^{13}\text{C}_4$ ]-Ret-regenerated Y185F-bR in the DA (blue) and M (red) states (E).

large downfield shifts of the  $^{13}\text{C}15$  and  $^{13}\text{C}14$  resonances in the M states may be the consequence of the conjugated Ret polyene chain breaking due to the deprotonation and access switch of the SB in the M states. These observations are consistent with the bond and torsion angle alternations extracted from the crystal structures of bR in the  $M_1$  and  $M_2$  states, which show a shortened C14–C15 bond and a heavily twisted C13=C14 bond (Fig. 1C-D) [37, 38]. Due to the attraction of the  $\pi$ -electrons along the conjugated polyene chain to the positively charged C13 site and movements of the aromatic rings of W182 and Y185 towards C11 in the M states, a striking upfield CS of C11 was observed in the M states [37, 38]. Fig. 2E shows the superimposed 2D  $^{13}\text{C}$ – $^{13}\text{C}$  PDSD correlation spectra of the [10, 11, 14, 15- $^{13}\text{C}_4$ ]-Ret-regenerated Y185F-bR in the DA (blue) state and M (red) states. The crosspeaks between the  $^{13}\text{C}15$  and  $^{13}\text{C}14$  resonances in the M states of the Y185F-bR were much less intense than those of the WT-bR, indicating that the formation of the M state in the Y185F-bR is more difficult than that in the WT-bR. The shift in the DA *cis-trans* isomerization equilibrium of the Ret chromophore due to the Y185F mutation might be the cause. By comparing the CSs of the Ret in WT-bR, large shifts of 2.2 ppm at C15, 0.8 ppm at C14, and –0.8 ppm at C11 were observed in  $\text{bR}_{cis}$ , but no apparent changes at those sites were identified in the  $\text{bR}_{trans}$  and M states (Table 1). These

observations suggested that the Ret and Y185 may be strongly coupled in the DA state with the aid of the phenolic hydroxyl of Y185.

In our previous studies, the CS of  $C\zeta^{Y185}$  (158 ppm) shifted farther downfield than the CS of  $C\zeta^{Y57}$  (155.8 ppm), and strong couplings between the C15 and C14 of Ret with Y185 were identified in the DA state, indicating that a SB N–H···OH–Y185 H-bond may exist between the Ret chromophore and Y185 [24]. Here, further 1D  $^{15}\text{N}$  CP experiments were performed on the  $^{15}\text{N}_2$ -K-labelled WT-bR and Y185F-bR to verify the existence of this SB N–H···OH–Y185 H-bond (Fig. S2). The CSs of the SB nitrogen in both  $bR_{cis}$  and  $bR_{trans}$  showed a large downfield shift in the Y185F-bR, suggesting that the positive charge on the SB nitrogen re-accumulates following the removal of the phenolic hydroxyl in the Y185F-bR, which clearly proved the possibility of the existence of this SB N–H···OH–Y185 H-bond. In addition, it has been classified that a strong to weak H-bond can form with a distance of 2.5-4.0 Å between X···A in a X–H···A–Y moiety in a biological system [60, 61]. Our automatic fragmentation quantum mechanics/molecular mechanics (AF-QM/MM) calculations [62-67] demonstrated that the calculated CS values at the C10, C11, C14 and C15 sites of the Ret chromophore and the SB nitrogen within a SB–N···O–Y185 distance of 3.1-3.3 Å match our ssNMR results very well in both  $bR_{cis}$  and  $bR_{trans}$ , as shown in Table S2 and Fig. S3.

**Table 1.** Chemical shift assignments of the [10, 11, 14, 15- $^{13}\text{C}_4$ ]-Ret-regenerated WT-bR and Y185F-bR in the DA and M states

	WT-bR				Y185F-bR			
	C10	C11	C14	C15	C10	C11	C14	C15
$bR_{cis}$ (DA)	130.0	139.0	110.0	163.2	130.0	138.0	111.8	165.4
$bR_{trans}$ (DA)	133.2	135.4	122.7	160.0	132.6	135.1	123.0	160.2
M <sub>1</sub> state	129.4		125.7	164.0	129.5		125.7	164.0
M <sub>2</sub> state	129.4		124.0	164.8	129.5		124.7	165.0

To explore the existence of the SB N–H···OH–Y185 H-bond upon bR activation, further 2D PDSD experiments were performed in the DA state and M states using

[U- $^{13}\text{C}_9$ ,  $^{15}\text{N}$ ]-Y-labelled WT-bR and [U- $^{13}\text{C}_9$ ,  $^{15}\text{N}$ ]-Y-[U- $^{13}\text{C}_9$ ,  $^{15}\text{N}$ ]-F-labelled Y185F-bR, regenerated with [10,11,14,15- $^{13}\text{C}_4$ ]-Ret. Fig. 3 presents comparisons of the 2D PDSD spectral regions of WT-bR and Y185F-bR in the DA state and M states, and the full sets of 2D PDSD spectra are shown in Figs. S4-5. Here, couplings among C14...C $\zeta^{\text{Y185}}$ , C15...C $\epsilon^{\text{Y185}}$  and C14...C $\epsilon^{\text{Y185}}$  in bR<sub>trans</sub>, and C14...C $\zeta^{\text{Y185}}$ , C14...C $\epsilon^{\text{Y185}}$  and C11...C $\epsilon^{\text{Y185}}$  in bR<sub>cis</sub> identified in the DA state of the WT-bR were not observed in the M states of the WT-bR and were also present in neither the DA state nor M states of the Y185F-bR, indicating that the N-H...OH-Y185 H-bond exists only in the DA WT-bR purple

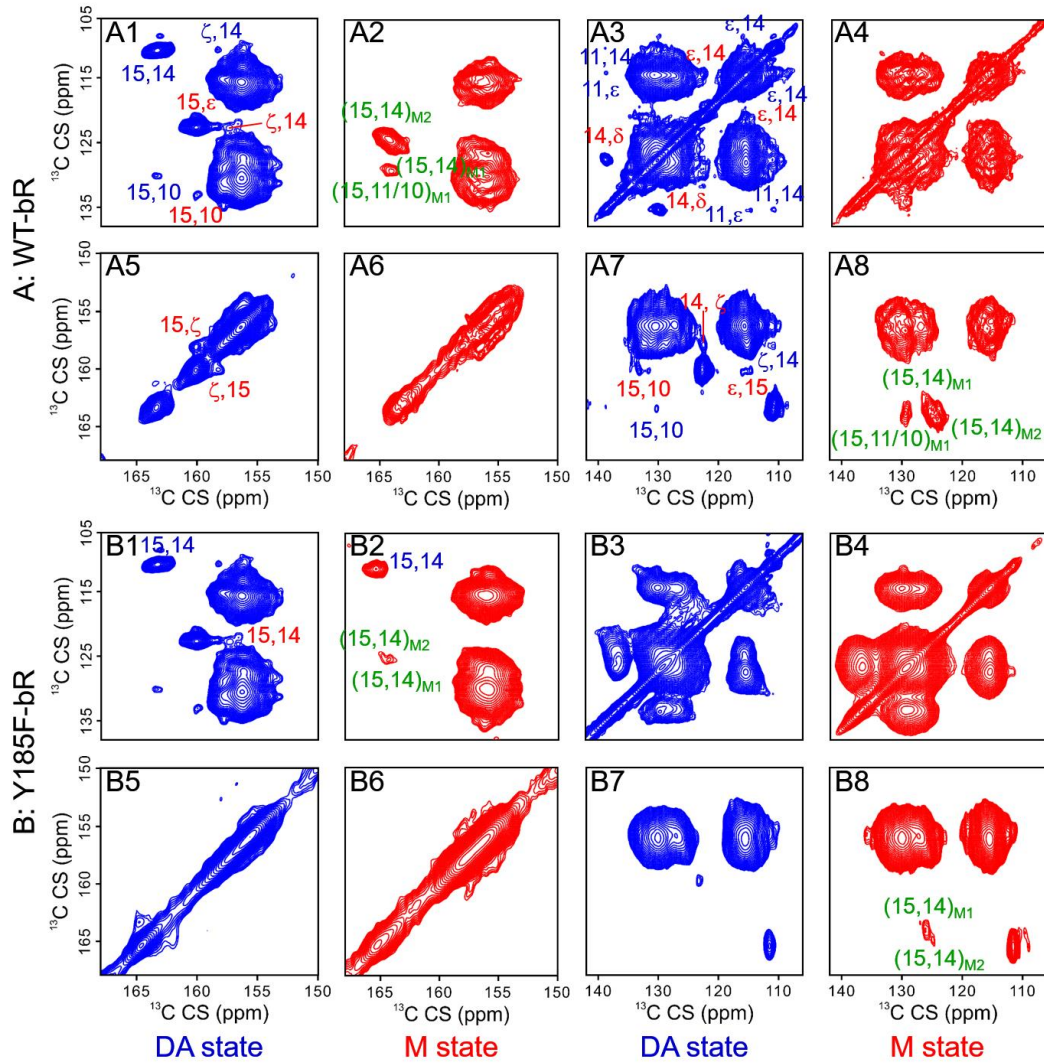


**Figure 3.** Regional 2D  $^{13}\text{C}$ - $^{13}\text{C}$  correlation spectra of the [U- $^{13}\text{C}_9$ ,  $^{15}\text{N}$ ]-Y-labelled WT-bR (panel A) and [U- $^{13}\text{C}_9$ ,  $^{15}\text{N}$ ]-Y-[U- $^{13}\text{C}_9$ ,  $^{15}\text{N}$ ]-F-labelled Y185F-bR (panel B) in the DA state and M states, and all the samples are all incorporated with [10, 11, 14, 15- $^{13}\text{C}_4$ ]-Ret. Contacts among C10, C11, C14 and C15 of the Ret and with Y185 are highlighted in blue for bR<sub>cis</sub> and red for bR<sub>trans</sub>, contacts among C10, C11, C14 and C15 of the Ret in the M states are highlighted in green.

membrane. Apart from the strong couplings formed by C15 and C14, a crosspeak was only observed at (164.0, 129.4) ppm, which can be attributed to the contact between C15 and both C11 and C10 in the M<sub>1</sub> state. However, no such crosspeak was identified in the M<sub>2</sub> state, indicating a more distorted 13-*cis* configuration in the M<sub>2</sub> state due to the access switch of the SB nitrogen [37, 38]. All the observations suggested that the SB N–H···OH–Y185 H-bond in the DA state is lost on conversion to the M states, accompanied by a drift of the aromatic ring of Y185 away from the Ret, and the couplings between the Y185 and Ret chromophore in the M states are much weaker than that in the DA state.

### 3.2 Mediation of Y185 in the photocycle kinetics in the bR purple membrane

The photo-isomerization of Ret from all-*trans* to 13-*cis*, 15-*anti* triggers a cyclic proton transfer reaction that includes a series of K-, L-, M-, N- and O-like photo-intermediates, and the influence of the removal of the SB N–H···OH–Y185 H-bond on the photocycle kinetics of bR can be studied by measuring the light-induced transient absorption changes in the M state at 410 nm and O state at 660 nm and in the recovery trajectory towards the ground state at 570 nm, as shown in Fig. 4A-B with the best-fitting values for the decay curves of each state listed in Table 2. Disturbed photocycle kinetics, particularly a weak and elongated decay of the M state and a prolonged recovery time towards the ground state, were observed in Y185F-bR. Again, this is in consistent with the observation of a much lower conversion of 13-*cis* during the light adaptation in the Y185F-bR by the <sup>15</sup>N CP experiments (Fig. S2 and Table S2). The curve at 660 nm represents a superimposed decay of the N state and rising and decay of the O state; no rising period was observed at 660 nm in Y185F-bR (Fig. 4B). Our results indicated that no O state forms in Y185F-bR, and the curve at 660 nm in Y185F-bR represents only the decay of the N state. Although an O-like species was reported in the Y185F-bR by FT-IR measurements [68-71], our 2D light-induced transient absorption change measurements further proved that the O state is missing in the photocycle of Y185F-bR, as shown in Fig. S6. A possible reason for the absence of this state might

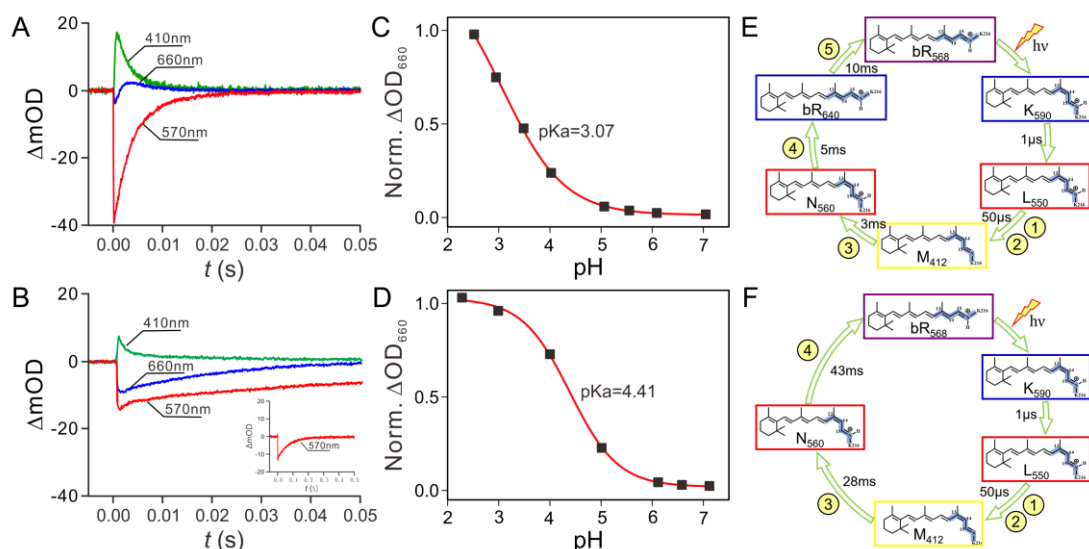


**Figure 4.** Light-induced transient absorption changes in the native membranes in the M and O states and the recovery trajectory towards the bR ground state at 410 nm, 660 nm, and 570 nm, respectively; WT-bR (A) and Y185F mutant (B). Complex titration curves of D85 of WT-bR and the Y185F mutant; WT-bR (C) and Y185F mutant (D). Photocycle of the WT-bR (E) and suggested photocycle of the Y185F mutant (F).

**Table 2.** Best fitting of the time constants of the photo-intermediate states at 410 nm, 660 nm and 570 nm for WT-bR and Y185F-bR

Sample	MS decay (ms)	OS rising (ms)	OS decay (ms)	Recovery to LAS (ms)
WT-bR	3.16	1.58	5.25	4.17
Y185F-bR	6.36	NA	NA	69.92

MS: M state; OS: O state; LAS: Light-adapted state.

be that the 13-*cis* domination after removal of the SB N–H···OH–Y185 H-bond impedes the formation of the all-*trans* Ret, which has been identified as the correct configuration in the O state in the crystal structure [72]. Compared with the photocycle of WT-bR, that of Y185F-bR appears to be deficient (Fig. 4E-F). The complex titration curve of D85 in the unphotolysed bR can be used to reveal the capability of the protonation of D85 and deprotonation of the SB during the photocycle after removal of the SB N–H···OH–Y185 H-bond [57]. The pKa value clearly increased by 1.4 units in the Y185F-bR (Fig. 4C-D and S7), indicating a weakened capability to accept a proton by D85 in the Y185F-bR. Our observations

suggested that removal of the SB N–H···OH–Y185 H-bond in the DA state not only alters the cavity of the Ret binding pocket to accommodate the *cis* configuration but also slows the dynamic conformational change of the binding pocket during the photocycle and alters the ability of the SB to transfer a proton transfer from SB to its acceptor, D85.

Our experiments provide the first evidence of the mediation mechanism of the Y185 on the bR photocycle through the SB N–H···OH–Y185 H-bond and explain why Y185 is involved in the reprotonation of the SB at the molecular level [21, 22, 73, 74]. Similar phenomena have been observed for other Ret binding residues in bR and other bacterial rhodopsins. Kouyama *et al.* reported that the M145F mutation in bR restrains the movement between the W182 and C13 methyl group of the Ret and further destabilizes the L state[75]. A 46-nm blue shift was observed in P206D-aSR, suggesting a redistribution of the electron along the Ret polyene chain and a deficient proton-pumping function [76]. The DA state of *Gloeobacter* rhodopsin contains primarily all-*trans* Ret in both alkaline and acidic forms and does not show appreciable signs of dark or light adaptation; however, replacement of E132Q has been shown to dramatically increase the 13-*cis* content of the DA state [77].

### **3.3 Mediation of Y185 in the purple membrane assembly dynamics and energy conversion in the *Halobacterium* strains**

bR forms a trimeric structure in the purple membrane [78], and the trimer-membrane interaction plays an important role in controlling the bR photocycle [56, 79]. Patch size and polydispersity indexes obtained by DLS have been used to determine protein assembly, dimerization and interactions under various conditions [80-82]. A single-peak distribution pattern with a narrower band for the WT-bR purple membrane and a broad band (large polydispersity indexes) for the Y185F L33 membrane were obtained at three different protein concentrations (Fig. 5A and Table 3), suggesting that the assembly dynamics of the purple membrane is altered in Y185F-bR. Although the ultrafast absorption and CD measurements suggested that the photocycle of the bR trimer in the purple membrane and bR

monomer in either Triton X-100 or the DMPC liposome are very similar and that monomeric bR is the functional unit, these studies either only focused on the very fast processes of the photocycle or did not measure the proton-pumping behaviour at 456 nm [83-85]. Disturbed photocycle kinetics, particularly a weak and elongated decay of the M state, a prolonged recovery time towards the ground state and a very weak or none O state were observed in the bR monomer in either Triton X-100 or the DMPC liposome in our studies (Fig. S8), and almost no proton-pumping capabilities were observed in the bR monomer in Triton X-100, DMPC liposome and DMPC nanodisc in our studies [86] (Fig. S9). Since the average particle sizes of the bR monomer vesicles are much smaller than those of the bR purple membrane (Table 3 and S3), our present studies clearly showed that the bR trimer with appropriate assembly dynamics is the basic functional unit for efficient proton pumping. The looser assembly dynamics observed in the Y185F-bR trimer may be the cause of the disturbed photocycle kinetics in the Y185F-bR.

*Halobacterium* employs its membrane-bound proton-pumping protein to synthesize adenosine triphosphate (ATP) under anaerobic conditions in the presence of light, thus forming ATP through photophosphorylation is directly correlated with the proton-pumping capability. Clearly, the ATP formation rate of the Y185F-bR in the L33 strain is lower than that of WT-bR in the R1M1 by almost one (Fig. 5B and S10). The highest ATP formation rate has been reported to be achieved when the light used is closest to the maximum absorption band (550-600 nm) of the Ret chromophore in the DA state of *Halobacterium* [87]. This wavelength band corresponds to the Ret isomerization thermal equilibrium at a 50:50 molar ratio [18]. In addition, our <sup>15</sup>N CP experiments of light-adapted (LA) WT-bR and Y185F-bR also showed that the conversion of 13-*cis* during the light adaptation is much lower in the Y185F-bR (Fig. S2 and Table S2). This observation supports our suggestion that maintaining the thermal equilibrium with a molar ratio between the 13-*cis* and all-*trans* isomers close to 1:1 in the DA purple membrane is crucial to maximizing ATP formation, since WT-bR has a maximum absorption at 555 nm with a molar ratio between the two isomers of nearly 1:1, and the Y185F-bR has a maximum



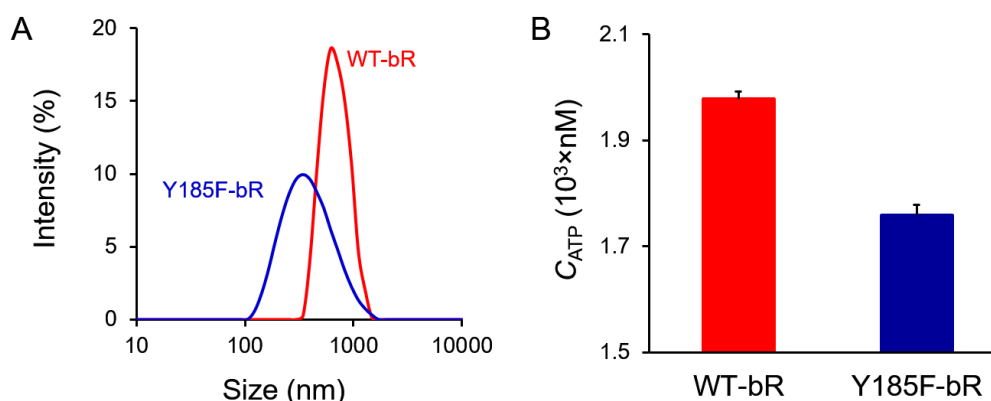


**Figure 5.** Patch size distributions of the WT-bR (R1M1) and Y185F-bR (L33) purple membrane fragments (A); ATP formation rates of the WT-bR in *Halobacterium* R1M1 and the Y185F-bR in *Halobacterium* L33 strains (B).

**Table 3.** Average particle sizes and polydispersity indexes of the WT-bR and Y185F-bR purple membrane fragments as measured by the DLS technique

Membrane fragments	Concentration (mM)	Average particle size (nm)	Polydispersity index
WT-bR	0.06	$635.8 \pm 3.7$	$0.156 \pm 0.009$
	0.08	$630.4 \pm 4.2$	$0.159 \pm 0.008$
	0.10	$627.6 \pm 3.5$	$0.150 \pm 0.005$
Y185F-bR	0.06	$346.7 \pm 9.9$	$0.244 \pm 0.017$
	0.08	$332.8 \pm 11.2$	$0.246 \pm 0.011$
	0.10	$336.7 \pm 5.9$	$0.230 \pm 0.013$

absorption at 548 nm with the 13-*cis* isomer as the dominant form in the DA state [16, 24]. Thus, the missing H-bond between the Y185 and SB can be assumed to not only affect the proton-pumping capability but also affect the assembly dynamics of the bR trimer in purple membranes and ATP formation. This hypothesis has been further verified by a low ATP formation in Archaeorhodopsin 4 (aR4), a bR-like proton pump, which has an all-*trans*-dominated isomer in its DA form [88, 89].

### 3.4 Functional role of Y185 as a rotamer switch controlling the bR photoactivation dynamics in the purple membrane

The protonated SB has access to the extracellular surface in the  $L \rightarrow M_1$  reaction to transfer a proton from the SB to the anionic D85. The unprotonated SB then switches access to the cytoplasmic surface to accept a proton from the initially

protonated D96 in the  $M_2 \rightarrow N$  reaction. Therefore, formation of the M states is crucial to completing the photocycle, and any different interaction mode between Y185 and the Ret chromophore in the M states will indicate a different rotamer conformation of the Y185. The SB  $N-H \cdots OH-Y185$  H-bond identified in the DA state and the couplings of  $C\zeta^{Y185}$  with C15 or C14 of Ret were not observed in the M states, thus suggesting a new rotamer conformation of the Y185 in the M states. In addition, other long-range contacts among C10, C11, C14 and C15 of the Ret and the aromatic ring of Y185 also disappeared due to the dynamic average of the dipolar couplings among them in the M states, suggesting a more flexible conformation in the M state than in the DA state. In the Y185-bR, a shifted Ret *cis-trans* isomerization thermal equilibrium, a deficient photocycle, and an unfavourable trimeric assembly dynamics and energy conversion were observed after removal of the phenolic hydroxyl of Y185. Clearly, Y185 may serve as a rotamer switch that retains the Ret *cis-trans* thermal equilibrium in the DA state and maintains the protein dynamics with a rigid conformation in the DA state through the SB  $N-H \cdots OH-Y185$  H-bond and a flexible conformation in the M states via release of this H-bond, and plays an important role in the directional transfer of the proton. This role is shown by the suggested structural model in Figure 6.

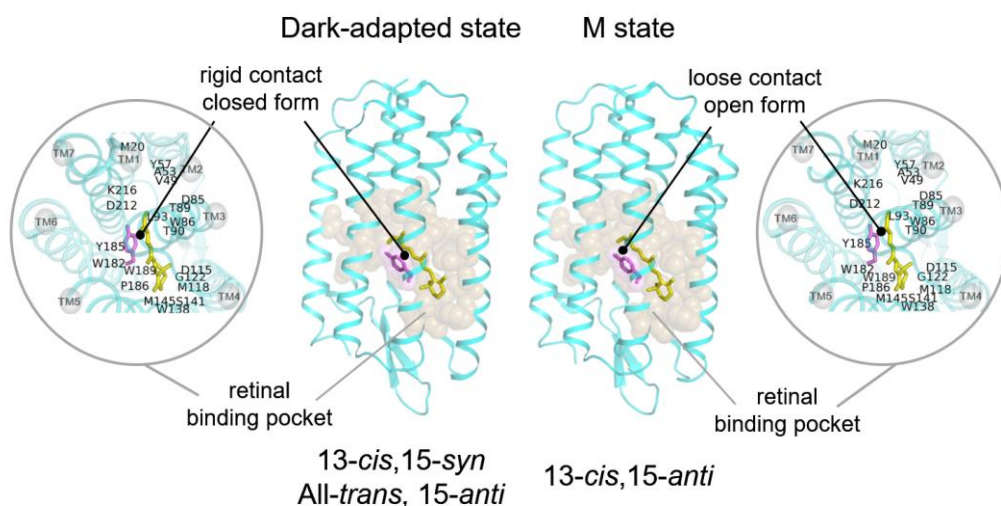


**Figure 6.** Structural model of Y185 serving as a rotamer switch to maintain the protein in a more rigid conformation for retaining the *cis-trans* thermal equilibrium of the Ret chromophore in the DA state and a more flexible conformation for more efficient directional transfer of the proton during the  $M_1 \rightarrow M_2$  reaction.

## 4. Conclusions

In summary, the functional roles of Y185 during the bR photocycle were studied systematically using *in situ* spectroscopies. A SB N–H···OH–Y185 H-bond was identified in the DA state and was lost upon conversion to the M states. Different interaction modes were identified between Y185 and the Ret chromophore in the DA state and M states. The couplings between the Y185 and Ret chromophore in the M states are more flexible than those in the DA state via release of the SB N–H···OH–Y185 H-bond and drift of the aromatic ring of Y185 away from the Ret. Y185 may serve as a rotamer switch, maintaining the protein dynamics for the efficient directional transfer of the proton. A shifted Ret *cis-trans* isomerization thermal equilibrium, a deficient photocycle, and unfavourable trimeric assembly dynamics and energy conversion were observed in the Y185F-bR after removal of the SB N–H···OH–Y185 H-bond.

## Conflict of interest

All authors claim that there are no conflicts of interest to declare.

## Acknowledgements

This research was supported by grants to X.Z. from the National Natural Science Foundation of China (grant numbers 30970657 and 21475045), the Shanghai Pujiang Program (grant number 09PJ1404300), and the East China Normal University (grant numbers 79003A29, 79301207, 79301411, and 41500-515430-14100) and by grants to A.W. from the Medical Research Council and Engineering and Physical Sciences Research Council of the UK and the State Administration of Foreign Experts Affairs of China through the High-End Foreign Experts Recruitment Program (GDW20123100086). Access to the EPSRC 850 MHz NMR facility is also acknowledged.

## References

- [1] D. Oesterhelt, W. Stoeckenius, Rhodopsin-like protein from the purple membrane of halobacterium halobium, *Nat. New Biol.*, 233 (1971) 149-152.

- [2] T. Friedrich, S. Geibel, R. Kalmbach, I. Chizhov, K. Ataka, J. Heberle, M. Engelhard, E. Bamberg, Proteorhodopsin is a light-driven proton pump with variable vectoriality, *J. Mol. Biol.*, 321 (2002) 821-838.
- [3] L. Vogeley, O.A. Sineshchekov, V.D. Trivedi, J. Sasaki, J.L. Spudich, H. Luecke, Anabaena sensory rhodopsin: A photochromic color sensor at 2.0 Å, *Science*, 306 (2004) 1390-1393.
- [4] M. Nack, I. Radu, C. Bamann, E. Bamberg, J. Heberle, The retinal structure of Channelrhodopsin-2 assessed by resonance raman spectroscopy, *FEBS Lett.*, 583 (2009) 3676-3680.
- [5] K. Ihara, T. Amemiya, Y. Miyashita, Y. Mukohata, Met-145 is a key residue in the dark adaptation of bacteriorhodopsin homologs, *Biophys. J.*, 67 (1994) 1187-1191.
- [6] K. Inoue, Y. Kato, H. Kandori, Light-driven ion-translocating rhodopsins in marine bacteria, *Trends Microbiol.*, 23 (2015) 91-98.
- [7] N. Enamil, K. Yoshimura, M. Murakami, H. Okumura, K. Hara, T. Kouyama, Crystal structures of Archaelhodopsin-1 and-2: Common structural motif in archaeal light-driven proton pumps, *J. Mol. Biol.*, 358 (2006) 675-685.
- [8] S.P. Balashov, E.S. Imasheva, V.A. Boichenko, J. Anton, J.M. Wang, J.K. Lanyi, Xanthorhodopsin: A proton pump with a light-harvesting carotenoid antenna, *Science*, 309 (2005) 2061-2064.
- [9] G. Varo, L. Zimanyi, X. Fan, L. Sun, R. Needleman, J.K. Lanyi, Photocycle of halorhodopsin from halobacterium salinarium, *Biophys. J.*, 68 (1995) 2062-2072.
- [10] O.P. Ernst, D.T. Lodowski, M. Elstner, P. Hegemann, L.S. Brown, H. Kandori, Microbial and animal rhodopsins: Structures, functions, and molecular mechanisms, *Chem. Rev.*, 114 (2014) 126-163.
- [11] F. Zhang, J. Vierock, O. Yizhar, L.E. Fenno, S. Tsunoda, A. Kianianmomeni, M. Prigge, A. Berndt, J. Cushman, J. Polle, J. Magnuson, P. Hegemann, K. Deisseroth, The microbial opsin family of optogenetic tools, *Cell*, 147 (2011) 1446-1457.
- [12] A.M. Ernst, B. Brügger, Sphingolipids as modulators of membrane proteins, *Biochim. Biophys. Acta*, 1841 (2014) 665-670.
- [13] J.K. Lanyi, A. Pohorille, Proton pumps: Mechanism of action and applications, *Trends Biotechnol.*, 19 (2001) 140-144.
- [14] J.K. Lanyi, Bacteriorhodopsin as a model for proton pumps, *Nature*, 375 (1995) 461-463.
- [15] D. Oesterhelt, M. Meentzen, L. Schuhmann, Reversible dissociation of the purple complex in bacteriorhodopsin and identification of 13-cis and all-trans-retinal as its chromophores, *Eur. J. Biochem.*, 40 (1973) 453-463.
- [16] W. Sperling, P. Carl, C.N. Rafferty, N.A. Dencher, Photochemistry and dark equilibrium of retinal isomers and bacteriorhodopsin isomers, *Biophys. Struct. Mech.*, 3 (1977) 79-94.
- [17] W. Stoeckenius, R.H. Lozier, R.A. Bogomolni, Bacteriorhodopsin and the purple membrane of halobacteria, *Biochim. Biophys. Acta*, 505 (1979) 215-278.
- [18] M. Tsuda, T.G. Ebrey, Effect of high pressure on the absorption spectrum and isomeric composition of bacteriorhodopsin, *Biophys. J.*, 30 (1980) 149-157.

- [19] G.S. Harbison, S.O. Smith, J.A. Pardo, C. Winkel, J. Lugtenburg, J. Herzfeld, R. Mathies, R.G. Griffin, Dark-adapted bacteriorhodopsin contains 13-cis, 15-syn and all-trans, 15-anti retinal schiff bases, *Proc. Natl. Acad. Sci. U. S. A.*, 81 (1984) 1706-1709.
- [20] J.K. Lanyi, Bacteriorhodopsin, *Annu. Rev. Physiol.*, 66 (2004) 665-688.
- [21] K.J. Rothschild, P. Roepe, P.L. Ahl, T.N. Earnest, R.A. Bogomolni, S.K. Das Gupta, C.M. Mulliken, J. Herzfeld, Evidence for a tyrosine protonation change during the primary phototransition of bacteriorhodopsin at low temperature, *Proc. Natl. Acad. Sci. U. S. A.*, 83 (1986) 347-351.
- [22] K. Rothschild, FTIR difference spectroscopy of bacteriorhodopsin: Toward a molecular model, *J. Bioenerg. Biomembr.*, 24 (1992) 147-167.
- [23] X. Ding, B. Peng, Y. Gao, H. Cui, D. Iuga, P. Judge, A. Watts, X. Zhao, Function of Tyr185 in stabilizing the isomerization equilibrium of the retinal chromophore in the bacteriorhodopsin ground state, *Biophys. J.*, 110 (2016) 377a.
- [24] X. Ding, H. Wang, B. Peng, H. Cui, Y. Gao, D. Iuga, P.J. Judge, G. Li, A. Watts, X. Zhao, Mediation mechanism of tyrosine 185 on the retinal isomerization equilibrium and the proton release channel in the seven-transmembrane receptor bacteriorhodopsin, *Biochim. Biophys. Acta*, 1857 (2016) 1786-1795.
- [25] T.W. Schwartz, T.M. Frimurer, B. Holst, M.M. Rosenkilde, C.E. Elling, Molecular mechanism of 7TM receptor activation - a global toggle switch model, *Annu. Rev. Pharmacol. Toxicol.*, 46 (2006) 481-519.
- [26] R. Nygaard, T.M. Frimurer, B. Holst, M.M. Rosenkilde, T.W. Schwartz, Ligand binding and micro-switches in 7TM receptor structures, *Trends Pharmacol. Sci.*, 30 (2009) 249-259.
- [27] A.Y.-H. Woo, K. Jozwiak, L. Toll, M.J. Tanga, J.A. Kozocas, L. Jimenez, Y. Huang, Y. Song, A. Plazinska, K. Pajak, R.K. Paul, M. Bernier, I.W. Wainer, R.-P. Xiao, Tyrosine 308 is necessary for ligand-directed Gs protein-biased signaling of  $\beta$ 2-adrenoceptor, *J. Biol. Chem.*, 289 (2014) 19351-19363.
- [28] A. Manglik, T.H. Kim, M. Masureel, C. Altenbach, Z. Yang, D. Hilger, M.T. Lerch, T.S. Kobilka, F.S. Thian, W.L. Hubbell, R.S. Prosser, B.K. Kobilka, Structural insights into the dynamic process of  $\beta$ 2-adrenergic receptor signaling, *Cell*, 161 (2015) 1101-1111.
- [29] A.J. Venkatakrishnan, X. Deupi, G. Lebon, C.G. Tate, G.F. Schertler, M.M. Babu, Molecular signatures of G-protein-coupled receptors, *Nature*, 494 (2013) 185-194.
- [30] K. Palczewski, T. Kumasaka, T. Hori, C.A. Behnke, H. Motoshima, B.A. Fox, I. Le Trong, D.C. Teller, T. Okada, R.E. Stenkamp, M. Yamamoto, M. Miyano, Crystal structure of rhodopsin: A G-protein-coupled receptor, *Science*, 289 (2000) 739-745.
- [31] V. Cherezov, D.M. Rosenbaum, M.A. Hanson, S.G.F. Rasmussen, F.S. Thian, T.S. Kobilka, H.J. Choi, P. Kuhn, W.I. Weis, B.K. Kobilka, R.C. Stevens, High-resolution crystal structure of an engineered human  $\beta$ 2-adrenergic G-protein-coupled receptor, *Science*, 318 (2007) 1258-1265.
- [32] V.P. Jaakola, M.T. Griffith, M.A. Hanson, V. Cherezov, E.Y.T. Chien, J.R. Lane, A.P. IJzerman, R.C. Stevens, The 2.6 angstrom crystal structure of a human  $A_{2a}$  adenosine receptor bound to an antagonist, *Science*, 322 (2008) 1211-1217.
- [33] M. Murakami, T. Kouyama, Crystal structure of squid rhodopsin, *Nature*, 453 (2008) 363-367.

- [34] D.M. Rosenbaum, V. Cherezov, M.A. Hanson, S.G.F. Rasmussen, F.S. Thian, T.S. Kobilka, H.-J. Choi, X.-J. Yao, W.I. Weis, R.C. Stevens, B.K. Kobilka, GPCR engineering yields high-resolution structural insights into  $\beta$ 2-adrenergic receptor function, *Science*, 318 (2007) 1266-1273.
- [35] T. Warne, M.J. Serrano-Vega, J.G. Baker, R. Moukhametzianov, P.C. Edwards, R. Henderson, A.G.W. Leslie, C.G. Tate, G.F.X. Schertler, Structure of a  $\beta$ 1-adrenergic G-protein-coupled receptor, *Nature*, 454 (2008) 486-492.
- [36] H. Luecke, B. Schobert, H.T. Richter, J.P. Cartailler, J.K. Lanyi, Structure of bacteriorhodopsin at 1.55 Å resolution, *J. Mol. Biol.*, 291 (1999) 899-911.
- [37] J.K. Lanyi, B. Schobert, Crystallographic structure of the retinal and the protein after deprotonation of the schiff base: The switch in the bacteriorhodopsin photocycle, *J. Mol. Biol.*, 321 (2002) 727-737.
- [38] H. Luecke, B. Schobert, J.P. Cartailler, H.T. Richter, A. Rosengarth, R. Needleman, J.K. Lanyi, Coupling photoisomerization of retinal to directional transport in bacteriorhodopsin, *J. Mol. Biol.*, 300 (2000) 1237-1255.
- [39] D. Oesterhelt, W. Stoerkenius, Isolation of the cell membrane of halobacterium halobium and its fractionation into red and purple membrane, *Methods Enzymol.*, 31 (1974) 667.
- [40] M.M. Bradford, A rapid and sensitive method for the quantitation of microgram quantities of protein utilizing the principle of protein-dye binding, *Anal. Biochem.*, 72 (1976) 248-254.
- [41] R.F. Shand, M.C. Betlach, Expression of the bop gene cluster of halobacterium halobium is induced by low oxygen tension and by light, *J. Bacteriol.*, 173 (1991) 4692-4699.
- [42] M. Rehorek, M.P. Heyn, Binding of all-trans-retinal to the purple membrane. Evidence for cooperativity and determination of the extinction coefficient, *Biochemistry*, 18 (1979) 4977-4983.
- [43] S.L. Helgerson, S.L. Siemsen, E.A. Dratz, Enrichment of bacteriorhodopsin with isotopically labeled amino acids by biosynthetic incorporation in halobacterium halobium, *Can. J. Microbiol.*, 38 (1992) 1181-1185.
- [44] G. Metz, X. Wu, S.O. Smith, Ramped-amplitude cross polarization in magic angle spinning NMR, *J. Magn. Reson. A*, 110 (1994) 219-227.
- [45] A.E. Bennett, C.M. Rienstra, M. Auger, K.V. Lakshmi, R.G. Griffin, Heteronuclear decoupling in rotating solids, *J. Chem. Phys.*, 103 (1995) 6951-6958.
- [46] N.M. Szeverenyi, M.J. Sullivan, G.E. Maciel, Observation of spin exchange by two-dimensional fourier transform  $^{13}\text{C}$  cross polarization-magic-angle spinning, *J. Magn. Reson.*, 47 (1982) 462-475.
- [47] K. Takegoshi, S. Nakamura, T. Terao,  $^{13}\text{C}$ - $^1\text{H}$  dipolar-assisted rotational resonance in magic-angle spinning NMR, *Chem. Phys. Lett.*, 344 (2001) 631-637.
- [48] M. Hohwy, H.J. Jakobsen, M. Eden, M.H. Levitt, N.C. Nielsen, Broadband dipolar recoupling in the nuclear magnetic resonance of rotating solids: A compensated C7 pulse sequence, *J. Chem. Phys.*, 108 (1998) 2686-2694.
- [49] M. Lee, W.I. Goldberg, Nuclear-magnetic-resonance line narrowing by a rotating rf field, *Phys. Rev.*, 140 (1965) A1261-A1271.

- [50] C.R. Morcombe, K.W. Zilm, Chemical shift referencing in MAS solid state NMR, *J. Magn. Reson.*, 162 (2003) 479-486.
- [51] L. Shi, M.A. Ahmed, W. Zhang, G. Whited, L.S. Brown, V. Ladizhansky, Three-dimensional solid-state NMR study of a seven-helical integral membrane proton pump--structural insights, *J. Mol. Biol.*, 386 (2009) 1078-1093.
- [52] J.G. Hu, B.Q. Sun, M. Bizounok, M.E. Hatcher, J.C. Lansing, J. Raap, P.J.E. Verdegem, J. Lugtenburg, R.G. Griffin, J. Herzfeld, Early and late M intermediates in the bacteriorhodopsin photocycle - A solid-state NMR study, *Biochemistry*, 37 (1998) 8088-8096.
- [53] J.C. Lansing, M. Hohwy, C.P. Jaroniec, A.F.L. Creemers, J. Lugtenburg, J. Herzfeld, R.G. Griffin, Chromophore distortions in the bacteriorhodopsin photocycle: Evolution of the H-C14-C15-H dihedral angle measured by solid-state NMR, *Biochemistry*, 41 (2002) 431-438.
- [54] M. Carravetta, X. Zhao, O.G. Johannessen, W.C. Lai, M.A. Verhoeven, P.H.M. Bovee-Geurts, P.J.E. Verdegem, S. Kiihne, H. Luthman, H.J.M. de Groot, W.J. deGrip, J. Lugtenburg, M.H. Levitt, Protein-induced bonding perturbation of the rhodopsin chromophore detected by double-quantum solid-state NMR, *J. Am. Chem. Soc.*, 126 (2004) 3948-3953.
- [55] Z. Cao, X. Ding, B. Peng, Y. Zhao, J. Ding, A. Watts, X. Zhao, Novel expression and characterization of a light driven proton pump archaerhodopsin 4 in a halobacterium salinarum strain, *Biochim. Biophys. Acta*, 1847 (2015) 390-398.
- [56] A.K. Mukhopadhyay, S. Bose, R.W. Hendler, Membrane-mediated control of the bacteriorhodopsin photocycle, *Biochemistry*, 33 (1994) 10889-10895.
- [57] S.P. Balashov, R. Govindjee, E.S. Imasheva, S. Misra, T.G. Ebrey, Y. Feng, R.K. Crouch, D.R. Menick, The two pKa's of aspartate-85 and control of thermal isomerization and proton release in the arginine-82 to lysine mutant of bacteriorhodopsin, *Biochemistry*, 34 (1995) 8820-8834.
- [58] G.E. Cullen, H.R. Keeler, H.W. Robinson, The pK' of the henderson-hasselbalch equation for hydrion concentration of serum, *J. Biol. Chem.*, 66 (1925) 301-322.
- [59] V.S. Bajaj, M.L. Mak-Jurkauskas, M. Belenky, J. Herzfeld, R.G. Griffin, Functional and shunt states of bacteriorhodopsin resolved by 250 GHz dynamic nuclear polarization-enhanced solid-state NMR, *Proc. Natl. Acad. Sci. U. S. A.*, 106 (2009) 9244-9249.
- [60] G.A. Jeffrey, *An introduction to hydrogen bonding*, Oxford University Press, Oxford, 1997.
- [61] G.R. Desiraju, T. Steiner, *The weak hydrogen bond in structural chemistry and biology*, Oxford University Press, Oxford, 1999.
- [62] X. He, B. Wang, K.M. Merz, Jr., Protein NMR chemical shift calculations based on the automated fragmentation QM/MM approach, *J. Phys. Chem. B*, 113 (2009) 10380-10388.
- [63] S. Tang, D.A. Case, Calculation of chemical shift anisotropy in proteins, *J. Biomol. NMR*, 51 (2011) 303-312.

- [64] T. Zhu, X. He, J.Z. Zhang, Fragment density functional theory calculation of NMR chemical shifts for proteins with implicit solvation, *Phys. Chem. Chem. Phys.*, 14 (2012) 7837-7845.
- [65] T. Zhu, J.Z. Zhang, X. He, Automated fragmentation QM/MM calculation of amide proton chemical shifts in proteins with explicit solvent model, *J. Chem. Theory Comput.*, 9 (2013) 2104-2114.
- [66] M.J. Frisch, G.W. Trucks, H.B. Schlegel, G.E. Scuseria, M.A. Robb, J.R. Cheeseman, G. Scalmani, V. Barone, B. Mennucci, G.A. Petersson, H. Nakatsuji, M. Caricato, Li, X., Hratchian, H. P., Izmaylov, A. F., Bloino, J., Zheng, G., Sonnenberg, J. L., Hada, M., Ehara, M., Toyota, K., Fukuda, R., Hasegawa, J., Ishida, M., Nakajima, T., Honda, Y., Kitao, O., Nakai, H., Vreven, T., Montgomery Jr., J. A., Peralta, J. E., Ogliaro, F., Bearpark, M. J., Heyd, J., Brothers, E. N., Kudin, K. N., Staroverov, V. N., Kobayashi, R., Normand, J., Raghavachari, K., Rendell, A. P., Burant, J. C., Iyengar, S. S., Tomasi, J., Cossi, M., Rega, N., Millam, N. J., Klene, M., Knox, J. E., Cross, J. B., Bakken, V., Adamo, C., Jaramillo, J., Gomperts, R., Stratmann, R. E., Yazyev, O., Austin, A. J., Cammi, R., Pomelli, C., Ochterski, J. W., Martin, R. L., Morokuma, K., Zakrzewski, V. G., Voth, G. A., Salvador, P., Dannenberg, J. J., Dapprich, S., Daniels, A. D., Farkas, Ö., Foresman, J. B., Ortiz, J. V., Cioslowski, J., and Fox, D. J., Gaussian 09 in, Gaussian, Inc., Wallingford, CT, 2009.
- [67] J.R. Cheeseman, G.W. Trucks, T.A. Keith, M.J. Frisch, A comparison of models for calculating nuclear magnetic resonance shielding tensors, *J. Chem. Phys.*, 104 (1996) 5497-5509.
- [68] P. Rath, M.P. Krebs, Y. He, H.G. Khorana, K.J. Rothschild, Fourier transform Raman spectroscopy of the bacteriorhodopsin mutant Tyr-185-->Phe: Formation of a stable O-like species during light adaptation and detection of its transient N-like photoproduct, *Biochemistry*, 32 (1993) 2272-2281.
- [69] O. Bousche, S. Sonar, M.P. Krebs, H.G. Khorana, K.J. Rothschild, Time-resolved fourier transform infrared spectroscopy of the bacteriorhodopsin mutant Tyr-185-->Phe: Asp-96 reprotonates during O formation; Asp-85 and Asp-212 deprotonate during O decay, *Photochem. Photobiol.*, 56 (1992) 1085-1095.
- [70] Y. He, M.P. Krebs, W.B. Fischer, H.G. Khorana, K.J. Rothschild, FTIR difference spectroscopy of the bacteriorhodopsin mutant Tyr-185-->Phe: Detection of a stable O-like species and characterization of its photocycle at low temperature, *Biochemistry*, 32 (1993) 2282-2290.
- [71] D.J. Jang, M.A. el-Sayed, L.J. Stern, T. Mogi, H.G. Khorana, Effect of genetic modification of tyrosine-185 on the proton pump and the blue-to-purple transition in bacteriorhodopsin, *Proc. Natl. Acad. Sci. U. S. A.*, 87 (1990) 4103-4107.
- [72] S. Rouhani, J.P. Cartailier, M.T. Facciotti, P. Walian, R. Needleman, J.K. Lanyi, R.M. Glaeser, H. Luecke, Crystal structure of the D85S mutant of bacteriorhodopsin: Model of an O-like photocycle intermediate, *J. Mol. Biol.*, 313 (2001) 615-628.
- [73] P.L. Ahl, L.J. Stern, D. Düring, T. Mogi, H.G. Khorana, K.J. Rothschild, Effects of amino acid substitutions in the F helix of bacteriorhodopsin. Low temperature ultraviolet/visible difference spectroscopy, *J. Biol. Chem.*, 263 (1988) 13594-13601.
- [74] M. Shibata, T. Tanimoto, H. Kandori, Water molecules in the schiff base region of bacteriorhodopsin, *J. Am. Chem. Soc.*, 125 (2003) 13312-13313.



- [75] T. Kouyama, R. Fujii, S. Kanada, T. Nakanishi, S.K. Chan, M. Murakami, Structure of archaerhodopsin-2 at 1.8 Å resolution, *Acta Crystallogr. D*, 70 (2014) 2692-2701.
- [76] A.R. Choi, S.Y. Kim, S.R. Yoon, K. Bae, K.H. Jung, Substitution of Pro206 and Ser86 residues in the retinal binding pocket of anabaena sensory rhodopsin is not sufficient for proton pumping function, *J. Microbiol. Biotechnol.*, 17 (2007) 138-145.
- [77] A.R. Choi, L. Shi, L.S. Brown, K.H. Jung, Cyanobacterial light-driven proton pump, gloeobacter rhodopsin: Complementarity between rhodopsin-based energy production and photosynthesis, *PLoS One*, 9 (2014) e110643.
- [78] R. Henderson, P.N.T. Unwin, Three-dimensional model of purple membrane obtained by electron microscopy, *Nature*, 257 (1975) 28-32.
- [79] A.K. Mukhopadhyay, S. Dracheva, S. Bose, R.W. Hendler, Control of the integral membrane proton pump, bacteriorhodopsin, by purple membrane lipids of halobacterium halobium, *Biochemistry*, 35 (1996) 9245-9252.
- [80] E. Ivanova, T.A. Jowitt, H. Lu, Assembly of the mitochondrial Tim9–Tim10 complex: A multi-step reaction with novel intermediates, *J. Mol. Biol.*, 375 (2008) 229-239.
- [81] A. Badarau, H. Rouha, S. Malafa, D.T. Logan, M. Hakansson, L. Stulik, I. Dolezilova, A. Teubenbacher, K. Gross, B. Maierhofer, S. Weber, M. Jagerhofer, D. Hoffman, E. Nagy, Structure-function analysis of heterodimer formation, oligomerization, and receptor binding of the staphylococcus aureus bi-component toxin lukgh, *J. Biol. Chem.*, 290 (2015) 142-156.
- [82] T. Janek, Z. Czyznikowska, J. Luczynski, E.J. Gudina, L.R. Rodrigues, J. Galezowska, Physicochemical study of biomolecular interactions between lysosomotropic surfactants and bovine serum albumin, *Colloids Surf. B. Biointerfaces*, 159 (2017) 750-758.
- [83] N.A. Dencher, M.P. Heyn, Bacteriorhodopsin monomers pump protons, *FEBS Lett.*, 108 (1979) 307-310.
- [84] J. Wang, M.A. El-Sayed, Time-resolved fourier transform infrared spectroscopy of the polarizable proton continua and the proton pump mechanism of bacteriorhodopsin, *Biophys. J.*, 80 (2001) 961-971.
- [85] J. Wang, M.A. El-Sayed, Time-resolved long-lived infrared emission from bacteriorhodopsin during its photocycle, *Biophys. J.*, 83 (2002) 1589-1594.
- [86] C. Liu (2014) Effects of different sample forms on NMR spectra resolution and protein dynamics. M. Sci. Master's thesis (East China Normal University, Shanghai).
- [87] J.M. Walter, D. Greenfield, C. Bustamante, J. Liphardt, Light-powering escherichia coli with proteorhodopsin, *Proc. Natl. Acad. Sci. U. S. A.*, 104 (2007) 2408-2412.
- [88] C. Sun, Y. Gao, X. Ding, X. Ding, J. Wang, J. Wang, H. Cui, H. Cui, Y. Yang, X. Zhao, Function of bacterioruberin in archaerhodopsin 4, from expression to characterization, *Biophys. J.*, 112 (2017) 571a-572a.
- [89] X.-Y. Ding, C. Sun, H.-L. Cui, Y.-J. Gao, J. Wang, Y.-N. Yang, F. Tian, X. Zhao, *In situ* solid-state NMR study of a new photoreceptor with two chromophores, *Eur. Biophys. J. Biophys.*, 46 (2017) S259.

# Supplementary material

## Functional roles of tyrosine 185 during the bacteriorhodopsin photocycle as revealed by *in situ* spectroscopic studies\*\*

Xiaoyan Ding<sup>1,2,‡</sup>, Chao Sun<sup>1,‡</sup>, Haolin Cui<sup>1</sup>, Sijin Chen<sup>1</sup>, Yujiao Gao<sup>1</sup>, Yanan Yang<sup>1</sup>, Juan Wang<sup>1</sup>, Xiao He<sup>3</sup>, Dinu Iuga<sup>4</sup>, Fang Tian<sup>2,\*</sup>, Anthony Watts<sup>5,\*</sup> and Xin Zhao<sup>1,\*</sup>

<sup>1</sup>Shanghai Key Laboratory of Magnetic Resonance, Department of Physics, East China Normal University, Shanghai 200062, P.R. China

<sup>2</sup>Department of Biochemistry and Molecular Biology, Penn State College of Medicine, PA 17033-0850, USA

<sup>3</sup>Department of Chemistry, East China Normal University, Shanghai 200062, P.R. China

<sup>4</sup>The UK 850 MHz Solid-State NMR Facility, Department of Physics, University of Warwick, Coventry CV4 7AL, UK

<sup>5</sup>Department of Biochemistry, University of Oxford, South Parks Road, Oxford OX1 3QU, UK

<sup>‡</sup>These authors contributed equally to this work.

\*Corresponding authors:

Shanghai Key Laboratory of Magnetic Resonance, Department of Physics; East China Normal University, Shanghai 200062, PR China. Tel.: +86-21-62234329; Fax: +86-21-62234329; Email: xzhao@phy.ecnu.edu.cn

Department of Biochemistry, University of Oxford, South Parks Road, Oxford OX1 3QU, UK. Tel.: +44-1865-613219; Fax: +44-1865-613201; Email: anthony.watts@bioch.ox.ac.uk

Department of Biochemistry and Molecular Biology, Penn State College of Medicine, PA 17033-0850, USA. Tel.: +1-717-531-8585; Fax: +1-717-531-7072; Email: ftian@psu.edu

## **<sup>15</sup>N CP experiments**

<sup>15</sup>N<sub>2</sub>-K-labelled bR purple membranes were prepared by using a synthetic medium [1] in which the unlabelled Lysine (K) was replaced by isotope <sup>15</sup>N-labelled K.

A ramped CP with a mixing time of 2 ms was used at an rf field of 50 kHz on the proton channel [2]. The two-pulse phase modulation (TPPM) [3] with a pulse width of 5.5-6 μs was used for proton decoupling. A MAS speed of 16 kHz and a recycle delay of 3 s were set for the experiments. The <sup>15</sup>N chemical shifts were referenced indirectly by using the gyromagnetic ratio of  $\gamma_N/\gamma_C=0.402979940$  [4].

## **Preparation of bR monomer in detergent**

The purple membrane fragments were suspended in a buffer with 0.1 M sodium acetate and 0.15 % Triton X-100 (w/v) at pH 5.0 in the dark for at least 48 hours at room temperature. The bR monomer was considered completely solubilized in Triton X-100 when no sediment appeared after 30 minutes of centrifugation at 45,000 × g, and the maximum absorption spectrum shifted from 568 to 553 nm. The concentration of the bR supernatant was adjusted at 568 nm to an OD of 1.0 using a 10-mm quartz cuvette [5, 6].

## **Reconstitution of bR in DMPC**

The bR Triton X-100 mixture was added to DMPC at a ratio of 1:4 (w/w) and then gently agitated for a few minutes to dissolve the DMPC, followed by dialysis against 0.1 M sodium acetate and 3 mM sodium azide at pH 5.0 in 4°C for 5 days to completely remove Triton X-100, and the supernatant was finally collected by centrifugation at 22,000 rpm [5].

All spectroscopic measurements were carried out at room temperature. The samples were adjusted to pH 7 and were converted into light-adapted forms before use.

## **Quantum mechanics/molecular mechanics calculations**

The chemical shifts of the Ret chromophore at the 10, 11, 14 and 15 sites were calculated using the automatic fragmentation quantum mechanics/molecular mechanics (AF-QM/MM) method [7]. Please refer to the publications by He *et al* for the accuracy and efficiency of this method [7-10]. Briefly, the whole protein was divided into three regions, the core region, buffer region and remaining region. The protonated Schiff base, including the Ret chromophore and K 216, is defined as the core region. The buffer region is defined by the residues within the retinal binding pocket and some other residues within 2.5 Å of the core region where the contacting atoms are hydrogen, and the residues within 4.0 Å where at least one of the contacting atoms is non-hydrogen. The remaining part of the protein is defined as the rest region. Both the core region and its buffer region were treated by quantum mechanics (QM) calculations, and the remaining region was calculated at the molecular mechanics (MM) level (as background charges). The chemical shifts were calculated by Gaussian 09 [11] using the GIAO [12] method at the B3LYP/6-31G\*\* level. The crystal structures of 1BRR and 1XOS are used as templates for the calculations.

## **2D light-induced transient absorption change spectroscopy**

The light-induced transient absorption changes were measured using a LP920 laser flash photolysis spectrometer (Edinburgh Instruments Ltd., Livingston, UK). The WT-bR and Y185F-bR purple membranes were excited with a light pulse at 532 nm, and the absorption was recorded in the time range from 0.0001 to 70 ms with a step of 10 ns and various wavelengths from 350 nm to 700 nm with a step of 10 nm. The absorption kinetics spectra were analysed using the photocycle kinetics model [13] through the singular value decomposition method [14]. The 2D absorption kinetics matrix measured at various times and wavelengths were decomposed into 4-5 major singular values, by which the sequential time-dependent spectra, each with its corresponding time constant and wavenumber, were determined using the MATLAB

program [15]. Clearly, the photocycle of WT-bR contains 4 components with maximum absorptions at 0.26  $\mu$ s, 3.39  $\mu$ s, 0.2 ms, and 2.9 ms, corresponding to wavelengths of 550 nm (L), 410 nm (M), 560 nm (N) and 640 nm (O), respectively (Fig. S6A). On the other hand, the photocycle of Y185F-bR shows only 3 components with maximum absorptions at 0.3  $\mu$ s, 3.47  $\mu$ s, and 0.14 ms corresponding to wavelengths of 550 nm (L), 410 nm (M) and 560 nm (N), respectively (Fig. S6B). Clearly, the O state is missing in the photocycle of Y185F-bR, indicating the influence of this mutation.

**Table S1.** Conservation of aromatic residues in microbial rhodopsin family proteins

No. in BR		42	57	79	83	86	138	182	185	189	208	219
H <sup>+</sup> pump	BR	F	Y	Y	Y	W	W	W	Y	W	F	F
	AR1	Y	Y	Y	Y	W	W	W	Y	W	F	F
	AR2	Y	Y	Y	Y	W	W	W	Y	W	F	F
	AR3	Y	Y	Y	Y	W	W	W	Y	W	F	F
	AR4	Y	Y	Y	Y	W	W	W	Y	W	F	F
	DR	F	Y	Y	Y	W	W	W	Y	W	F	F
	LR	Y	Y	Y	Y	W	Y	W	Y	W	Y	F
	CR1	F	Y	Y	Y	W	W	W	Y	W	F	F
	CR2	F	Y	Y	Y	W	W	W	Y	W	F	F
	CR3	F	Y	Y	Y	W	W	W	Y	W	F	F
	MR	Y	Y	Y	Y	W	W	W	Y	W	Y	F
	LR	Y	Y	Y	Y	W	Y	W	Y	W	Y	F
	PH2	L	Y	F	Y	W	V	W	Y	W	Y	F
	NR	F	Y	F	Y	W	Y	W	Y	W	Y	F
	PH1	F	Y	Y	Y	W	F	W	Y	W	Y	F
	Ace1	-	Y	I	Y	W	F	W	Y	W	M	Y
	Ace2	A	Y	Y	Y	W	F	W	Y	W	M	F
	GR	-	-	-	Y	W	G	W	Y	Y	Y	F
	XR	-	-	-	Y	W	G	W	Y	Y	Y	Y
	KR1	-	-	F	Y	W	G	W	Y	Y	Y	F
	GPR1	-	-	-	Y	W	G	W	Y	Y	Y	F
	BPR4	-	-	-	Y	W	-	W	Y	Y	Y	F
	GPR2	S	Y	Y	Y	W	F	W	Y	Y	Y	F
	GPR3	-	Y	Y	Y	W	F	W	Y	Y	Y	F
	GPR6	S	Y	F	Y	W	-	W	Y	Y	Y	F
	GPR7	S	Y	F	Y	W	-	W	Y	Y	Y	F
	BPR5	S	Y	F	Y	W	-	W	Y	Y	Y	F
Na <sup>+</sup> pump	KR2	-	V	Y	Y	W	G	W	Y	Y	Y	Y
	NaR	-	-	-	Y	W	G	W	Y	Y	Y	Y
Cl <sup>-</sup> pump	HR	I	Y	Q	Y	W	Y	W	Y	W	Y	F
	NpHR	I	Y	M	Y	W	Y	W	Y	W	Y	F
	SrHR	I	Y	L	Y	W	Y	W	Y	W	Y	F
Channel	CrChR1	-	-	V	Y	W	F	W	F	F	H	W
	CrChR2	-	-	Q	Y	W	G	W	F	F	H	W
	MvChR1	-	-	-	Y	W	Y	W	F	P	H	W
	VcChR1	-	-	V	Y	W	F	W	F	F	H	W
	VcChR2	-	-	L	Y	W	G	W	F	F	H	W
Sensor	HsSRII	Y	Y	Y	Y	W	F	W	Y	W	V	F
	HvSRI	I	Y	G	Y	W	F	W	Y	W	Y	Y
	HvSRII	R	Y	Y	Y	W	F	W	Y	W	V	F
	NpSRII	Y	Y	F	Y	W	F	W	Y	W	I	F

**Table S2.** 13-*cis* to all-*trans* ratio of the Ret in the DA WT-bR and Y185F-bR native membranes, and the conversion rate of 13-*cis* to all-*trans* upon illumination at 0°C for 3 hours as measured by <sup>15</sup>N CP-MAS experiments

	13- <i>cis</i> :all- <i>trans</i>	Conversion rate of 13- <i>cis</i> (%)
WT-bR	52:48	80
Y185F-bR	78:22	28

**Table S3.** Comparison of the chemical shifts of C10, C11, C14 and C15 of the Ret chromophore and SB nitrogen in the WT-bR as determined by ssNMR and calculated by the AF-QM/MM method\*

	ssNMR					AF-QM/MM				
	C10	C11	C14	C15	N <sub>SB</sub>	C10	C11	C14	C15	N <sub>SB</sub>
bR <sub>cis</sub>	130.0	139.0	110.0	163.2	176.0	129.6	139.0	109.9	163.1	175.5
bR <sub>trans</sub>	133.2	135.4	122.7	160.0	168.9	132.8	135.2	122.3	159.6	168.7

\*RMSD of the calculation is 0.280 for bR<sub>cis</sub> and 0.378 for bR<sub>trans</sub>.

**Table S4.** Dynamic light scattering measurements of the WT-bR in Triton X-100 and DMPC liposomes

Sample	Concentration (mM)	Average particle size (nm)	Polydispersity index
WT-bR in Triton X-100	0.06	32.3±3.2	0.352±0.0291
	0.08	30.5±0.7	0.360±0.0200
	0.10	25.7±4.6	0.357±0.0111
WT-bR in DMPC	0.06	187.1±1.2	0.083±0.0070
	0.08	188.4±0.8	0.077±0.0180
	0.10	187.8±2.1	0.068±0.0318

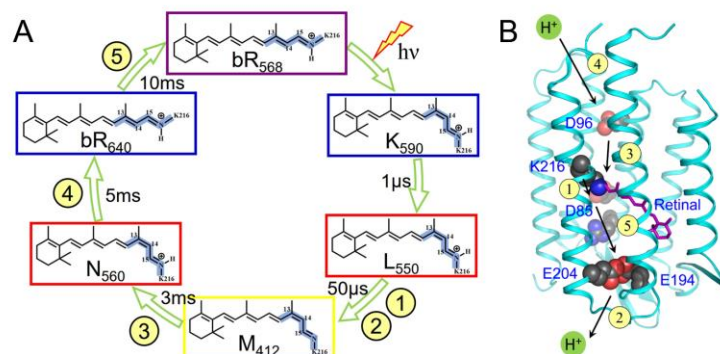


**Figure S1.** bR photocycle (A); the five vectorial transfer steps of a proton across the membrane during the photocycle (B).

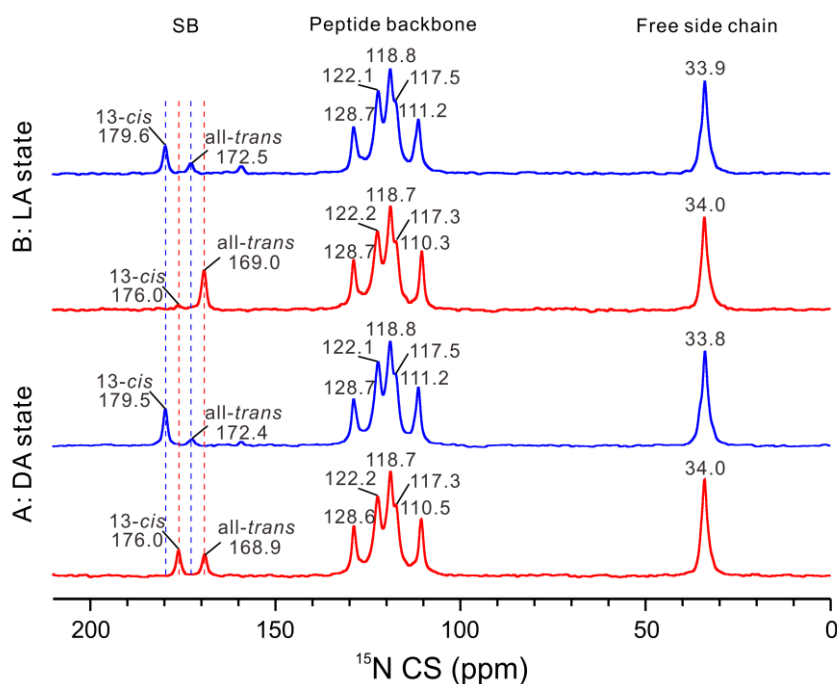


**Figure S2.** <sup>15</sup>N CP spectra of the <sup>15</sup>N<sub>2</sub>-K-labelled WT-bR (red), and Y185F-bR (blue) in DA state (A), and LA state (B) with a CP mixing time of 2 ms, and a MAS speed of 16 kHz.

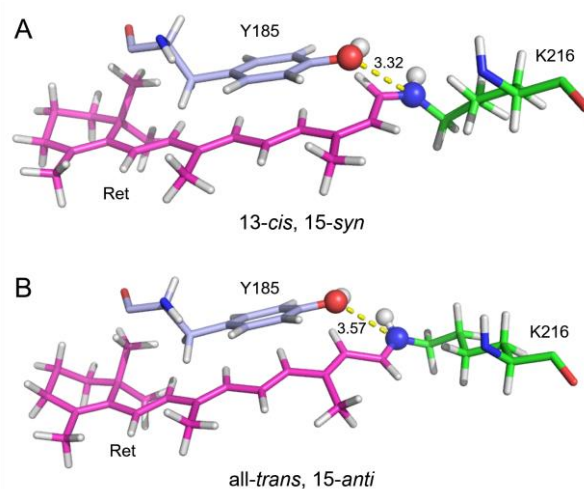


**Figure S3.** AF-QM/MM calculations of the interaction between Y185 and based on the CS values of bR<sub>cis</sub>, bR<sub>trans</sub> and the SB nitrogen. A: 13-cis, 15-syn; B: all-trans, 15-anti.



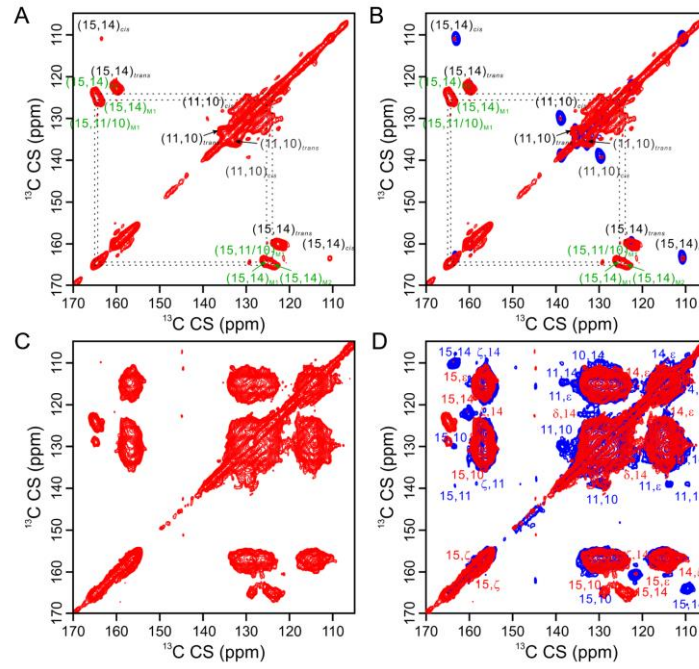


**Figure S4.** A: 2D  $^{13}\text{C}$ – $^{13}\text{C}$  PDS correlation spectra of the WT  $^{13}\text{C}_4$ -Ret-bR purple membranes in the M state; B: superimposition of the  $^{13}\text{C}_4$ -Ret-bR correlation spectra of the M state (red) with the DA state (blue); C: 2D  $^{13}\text{C}$ – $^{13}\text{C}$  PDS correlation spectra of the WT  $^{13}\text{C}_4$ -Ret- $^{13}\text{C}_9$ -Y-bR purple membranes in the M state; D: superimposition of the  $^{13}\text{C}_4$ -Ret- $^{13}\text{C}_9$ -Y-bR correlation spectra of the M state (red) with the DA state (blue).

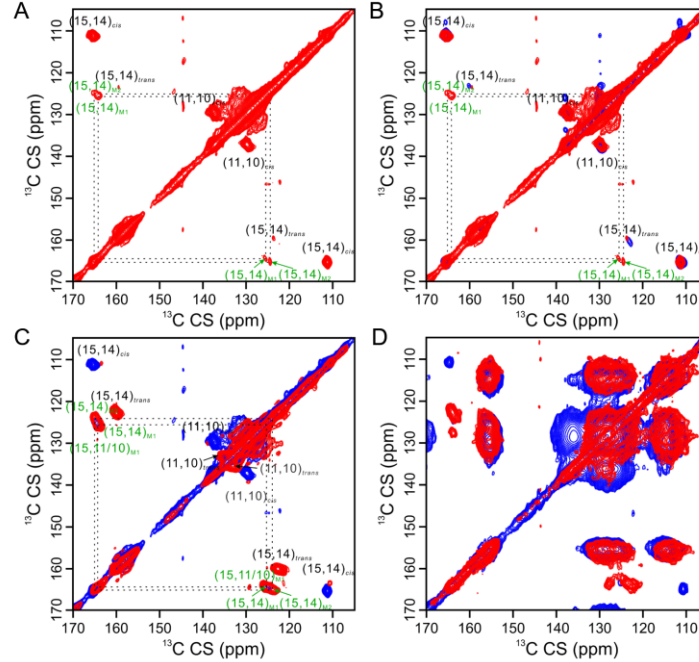


**Figure S5.** A: 2D  $^{13}\text{C}$ – $^{13}\text{C}$  PDS correlation spectra of the  $^{13}\text{C}_4$ -Ret-Y185F-bR in the M state; B: superimposition of the  $^{13}\text{C}_4$ -Ret-Y185F-bR correlation spectra of the M state (red) with the DA state (blue); C: superimposition of the correlation spectra of the WT  $^{13}\text{C}_4$ -Ret-bR (red) with the  $^{13}\text{C}_4$ -Ret-Y185F mutant (blue) in the M state; D: superimposition of the correlation spectra of the WT  $^{13}\text{C}_4$ -Ret- $^{13}\text{C}_9$ -Y-bR (red) with the  $^{13}\text{C}_4$ -Ret- $^{13}\text{C}_9$ -Y- $^{13}\text{C}_9$ -F-Y185F mutant (blue) in the M state.

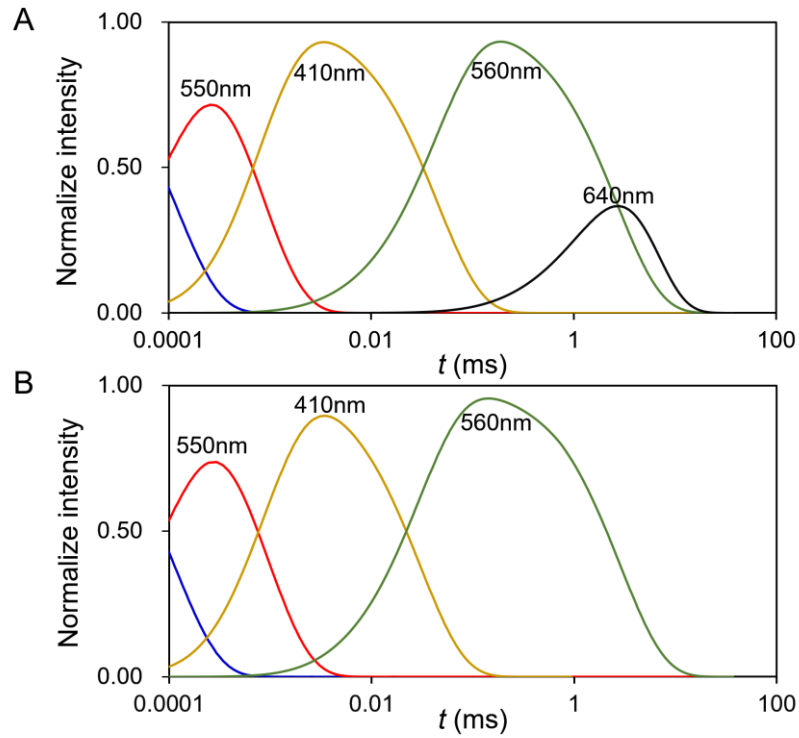


**Figure S6.** Best-fitting curves according to the singular-value decomposition of the 2D absorption kinetics matrix of the WT-bR (A) and Y185F-bR (B) purple membranes in 100 mM NaCl and 20 mM KCl at pH 7.0.

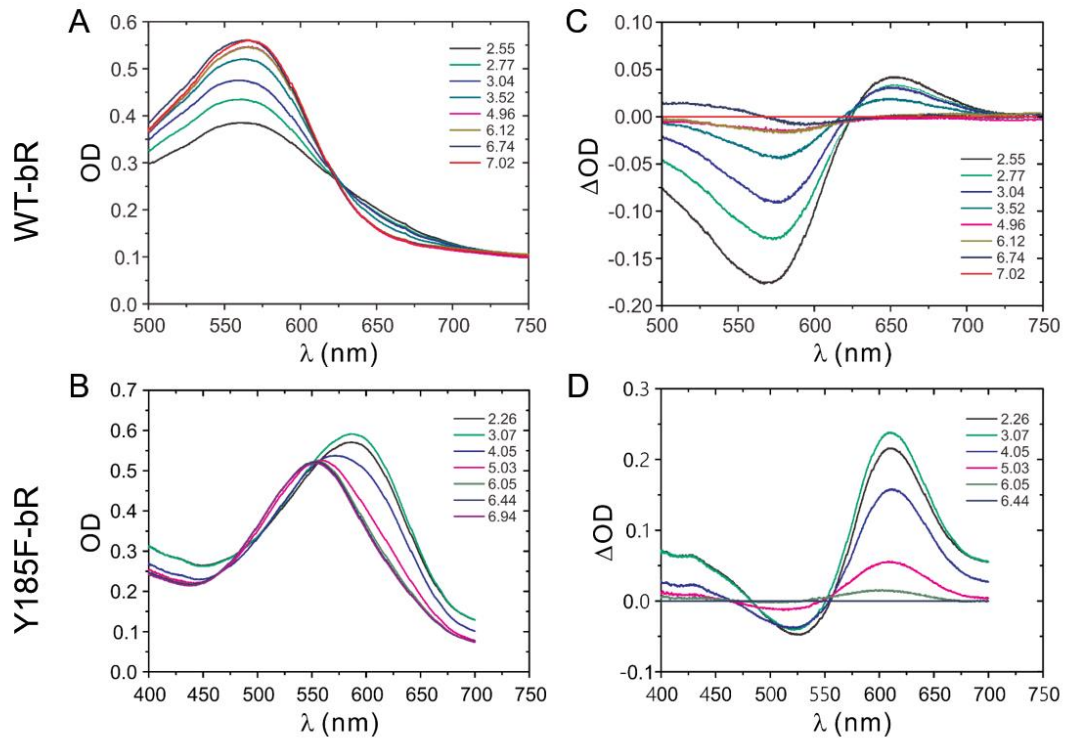


**Figure S7.** Complex titration curves of D85 of WT-bR and the Y185F-bR in the unphotolysed native membranes. A and B: pH-dependent absorption spectra of WT-bR and the Y185F-bR, respectively; C and D: differences obtained by subtracting the last spectrum in A and C, respectively.

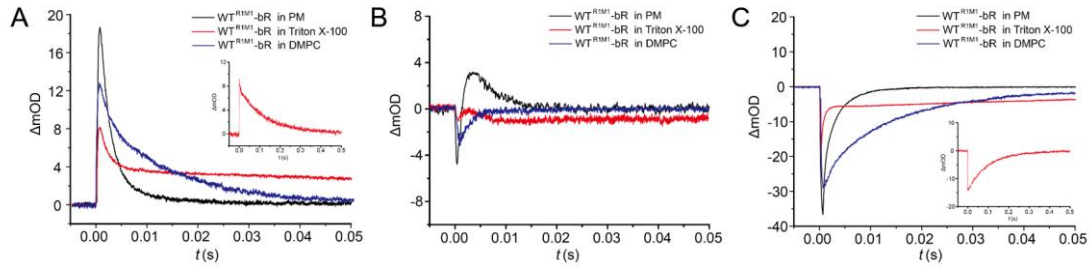


**Figure S8.** Light-induced transient absorption changes of bR in purple membranes, Triton X-100 and DMPC liposomes at A: 410 nm (M state); B: 660 nm (O state); C: 570 nm (recovery trajectory towards the bR ground state), respectively.

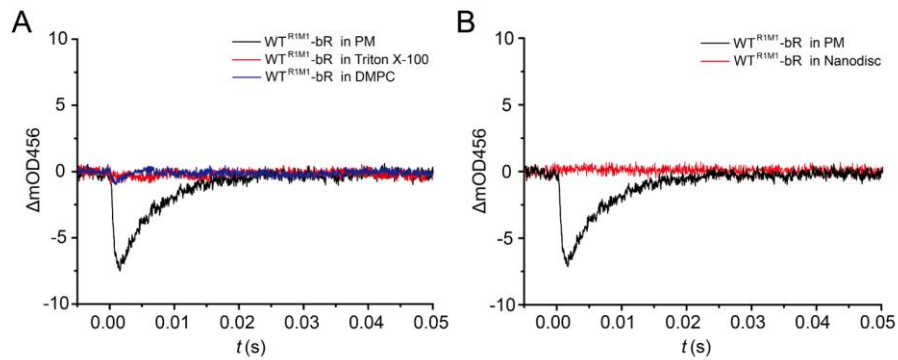


**Figure S9.** Comparison of the proton-pumping capability of bR at 456 nm. A: in purple membranes, Triton X-100 and DMPC liposomes; B: in purple membranes and DMPC nanodisc [16].

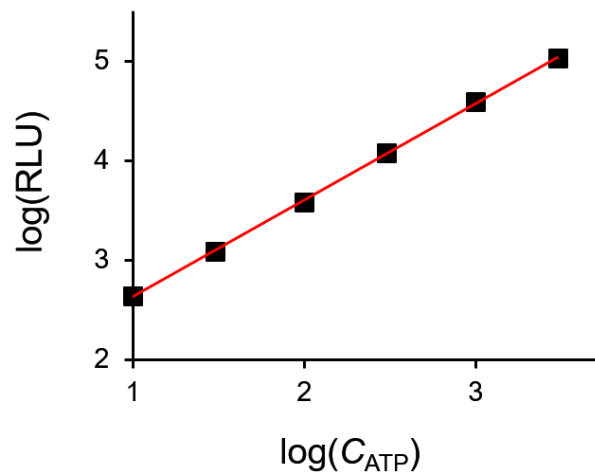


**Figure S10.** Calibration of the ATP concentration with the best-fitting curve of  $\log(RLU) = 0.93968 \times \log(C_{ATP}) + 1.72045$ ,  $R^2=0.99767$ .

## References

- [1] X. Ding, H. Wang, B. Peng, H. Cui, Y. Gao, D. Iuga, P.J. Judge, G. Li, A. Watts, X. Zhao, Mediation mechanism of tyrosine 185 on the retinal isomerization equilibrium and the proton release channel in the seven-transmembrane receptor bacteriorhodopsin, *Biochim. Biophys. Acta*, 1857 (2016) 1786-1795.
- [2] G. Metz, X. Wu, S.O. Smith, Ramped-amplitude cross polarization in magic angle spinning NMR, *J. Magn. Reson. A*, 110 (1994) 219-227.
- [3] A.E. Bennett, C.M. Rienstra, M. Auger, K.V. Lakshmi, R.G. Griffin, Heteronuclear decoupling in rotating solids, *J. Chem. Phys.*, 103 (1995) 6951-6958.
- [4] L. Shi, M.A. Ahmed, W. Zhang, G. Whited, L.S. Brown, V. Ladizhansky, Three-dimensional solid-state NMR study of a seven-helical integral membrane proton pump--structural insights, *J. Mol. Biol.*, 386 (2009) 1078-1093.
- [5] R.J. Cherry, U. Müller, R. Henderson, M.P. Heyn, Temperature-dependent aggregation of bacteriorhodopsin in dipalmitoyl- and dimyristoylphosphatidylcholine vesicles, *J. Mol. Biol.*, 121 (1978) 283-298.
- [6] J.P. Wang, S. Link, C.D. Heyes, M.A. El-Sayed, Comparison of the dynamics of the primary events of bacteriorhodopsin in its trimeric and monomeric states, *Biophys. J.*, 83 (2002) 1557-1566.
- [7] X. He, B. Wang, K.M. Merz, Jr., Protein NMR chemical shift calculations based on the automated fragmentation QM/MM approach, *J. Phys. Chem. B*, 113 (2009) 10380-10388.
- [8] T. Zhu, X. He, J.Z.H. Zhang, Fragment density functional theory calculation of NMR chemical shifts for proteins with implicit solvation, *Phys. Chem. Chem. Phys.*, 14 (2012) 7837-7845.
- [9] S. Tang, D.A. Case, Calculation of chemical shift anisotropy in proteins, *J. Biomol. NMR*, 51 (2011) 303-312.
- [10] T. Zhu, J.Z. Zhang, X. He, Automated fragmentation QM/MM calculation of amide proton chemical shifts in proteins with explicit solvent model, *J. Chem. Theory Comput.*, 9 (2013) 2104-2114.
- [11] M.J. Frisch, G.W. Trucks, H.B. Schlegel, G.E. Scuseria, M.A. Robb, J.R. Cheeseman, G. Scalmani, V. Barone, B. Mennucci, G.A. Petersson, H. Nakatsuji, M. Caricato, Li, X., Hratchian, H. P., Izmaylov, A. F., Bloino, J., Zheng, G., Sonnenberg, J. L., Hada, M., Ehara, M., Toyota, K., Fukuda, R., Hasegawa, J., Ishida, M., Nakajima, T., Honda, Y., Kitao, O., Nakai, H., Vreven, T., Montgomery Jr., J. A., Peralta, J. E., Ogliaro, F., Bearpark, M. J., Heyd, J., Brothers, E. N., Kudin, K. N., Staroverov, V. N., Kobayashi, R., Normand, J., Raghavachari, K., Rendell, A. P., Burant, J. C., Iyengar, S. S., Tomasi, J., Cossi, M., Rega, N., Millam, N. J., Klene, M., Knox, J. E., Cross, J. B., Bakken, V., Adamo, C., Jaramillo, J., Gomperts, R., Stratmann, R. E., Yazyev, O., Austin, A. J., Cammi, R., Pomelli, C., Ochterski, J. W., Martin, R. L., Morokuma, K., Zakrzewski, V. G., Voth, G. A., Salvador, P., Dannenberg, J. J., Dapprich, S., Daniels, A. D., Farkas, Ö., Foresman, J. B., Ortiz, J. V., Cioslowski, J., and Fox, D. J., *Gaussian 09* in, Gaussian, Inc., Wallingford, CT, 2009.
- [12] J.R. Cheeseman, G.W. Trucks, T.A. Keith, M.J. Frisch, A comparison of models for calculating nuclear magnetic resonance shielding tensors, *J. Chem. Phys.*, 104 (1996)

5497-5509.

- [13] I. Chizhov, D.S. Chernavskii, M. Engelhard, K.H. Mueller, B.V. Zubov, B. Hess, Spectrally silent transitions in the bacteriorhodopsin photocycle, *Biophys. J.*, 71 (1996) 2329-2345.
- [14] E.R. Henry, J. Hofrichter, Singular value decomposition: Application to analysis of experimental data, in: *Methods enzymol.*, Academic Press, 1992, pp. 129-192.
- [15] L.J. van Wilderen, C.N. Lincoln, J.J. van Thor, Modelling multi-pulse population dynamics from ultrafast spectroscopy, *PLoS One*, 6 (2011) e17373.
- [16] C. Liu (2014) Effects of different sample forms on NMR spectra resolution and protein dynamics. M. Sci. Master's thesis (East China Normal University, Shanghai).